Reducible Fermi surface for multi-layer quantum graphs including stacked graphene

Lee Fisher[1] and Wei Li[2] and Stephen P. Shipman[3]

Departments of Mathematics
University of California at Irvine[1], DePaul University[2], Louisiana State University[3]

Abstract. We construct two types of multi-layer quantum graphs (Schrödinger operators on metric graphs) for which the dispersion function of wave vector and energy is proved to be a polynomial in the dispersion function of the single layer. This leads to the reducibility of the algebraic Fermi surface, at any energy, into several components. Each component contributes a set of bands to the spectrum of the graph operator. When the layers are graphene, AA-, AB-, and ABC-stacking are allowed within the same multi-layer structure. One of the tools we introduce is a surgery-type calculus for obtaining the dispersion function for a periodic quantum graph by joining two graphs together. Reducibility of the Fermi surface allows for the construction of local defects that engender bound states at energies embedded in the radiation continuum.

Key words: multi-layer structure, quantum graph, periodic operator, reducible Fermi surface, Floquet transform, graphene, Dirac cone, conical singularity, embedded eigenvalue

MSC: 47A75, 47B25, 39A70, 39A14, 47B39, 47B40, 39A12

1 Introduction

The Fermi surface of a d-periodic operator at an energy λ is the set of wavevectors $(k_1, \dots, k_d)$ admissible by the operator at that energy. It is the zero-set of the dispersion function $D(k_1, \dots, k_d, \lambda)$, and for periodic graph operators, this is a Laurent polynomial in the Floquet variables $(z_1, \dots, z_d) = (e^{ik_1}, \dots, e^{ik_d})$. When the dispersion function can be factored, for each fixed energy, as a product of two or more polynomials in $(z_1, \dots, z_d)$, each irreducible component contributes a sequence of spectral bands and gaps. Reducibility is required for the existence of embedded eigenvalues engendered by a local defect [39, 40], except for the anomalous situation when an eigenfunction has compact support.

Irreducibility appears to be generic in the sense that a polynomial in several variables is generically not factorable into nonconstant polynomials of lower degree—factorability requires the coefficients of the polynomial to lie on a certain algebraic variety in coefficient space. Thus it is natural that proofs of reducibility rely on specific constructions that are tailored to result in factorability of the dispersion function. This work describes two such constructions. On the other hand, proofs of irreducibility invoke more *ad hoc* methods. Let us first briefly describe the known results on (ir)reducibility.

[1]UC @ Irvine, fisherla525@gmail.com
[2]DePaul University, Chicago, wei.li@depaul.edu
[3]LSU @ Baton Rouge, shipman@lsu.edu, ORCID 0000-0001-6620-6528

Irreducibility of the Fermi surface is known to occur for the discrete Laplace operator plus a periodic potential in any dimension. This was proved in two and three dimensions in [6],[31, Ch. 4],[7, Theorem 2] for all but finitely many energies, and recently for all energies in dimension higher than two [46]. Proofs rely on the algebraic structure arising from the relative simplicity of the discrete Laplacian on a square graph. Irreducibility is also known for the continuous Laplacian in three dimensions plus a periodic potential of the form $q_1(x_1)+q_2(x_2,x_3)$ [8, Sec. 2]. Irreducibility for all but finitely many energies is established for discrete graph Laplacians with positive weights and more general graph operators, where the underlying graph is planar with two vertices per period [44]. The proof is purely computational.

All constructions so far of graph operators with reducible Fermi surface involve multiple coupled layers [59, 60]. The simplest are constructed by coupling several identical copies of a discrete graph operator, using Hermitian coupling constants [59, §2]; or by coupling two identical layers of a quantum graph by edges between corresponding vertices, where the potential $q_e(x)$ of the Schrödinger operator $-d^2/dx^2 + q_e(x)$ on each coupling edge e is symmetric about the center of the edge [59, §3]. When the layers are not coupled symmetrically, a compatibility condition for the potentials on the coupling edges, which is sufficient for reducibility, was proved in [60, Theorem 4]. The condition involves a certain "spectral asymmetry function" $a_{q_e}(\lambda)$ depending on the potential $q_e(x)$, which is defined in that article. Two potentials $q_{e_1}(x)$ and $q_{e_2}(x)$ are compatible if their spectral asymmetry functions are identical. It turns out that each class of compatible potentials, corresponding to a given asymmetry function $a(\lambda)$, contains exactly one square-integrable potential for each admissible Dirichlet spectral sequence [13].

The present work introduces two new classes of self-adjoint periodic multi-layer quantum graph operators with reducible Fermi surface. For both types, several layers are connected at corresponding vertices by general graphs, as illustrated in Fig. 1. Reducibility results from a different mechanism from [60], namely that the dispersion function of the multi-layer graph turns out to be a polynomial function of a "composite Floquet variable" $\zeta(z_1,\dots,z_d,\lambda)$,

$$D(z_1,\dots,z_d,\lambda) \;=\; P\big(\zeta(z_1,\dots,z_d,\lambda),\lambda\big).$$

The function ζ is a Laurent polynomial in $(z_1,\dots,z_d)$ with coefficients that are meromorphic in λ; and P is a polynomial in ζ with coefficients that are meromorphic in λ. The components of the Fermi surface at energy λ are therefore of the form $\zeta(z_1,\dots,z_d;\lambda)=\rho(\lambda)$, where $\rho(\lambda)$ is one of the roots of $P(\zeta,\lambda)$ as a polynomial in ζ.

Here is a summary of properties of the two types of multi-layer quantum graphs, introduced in this work, that have reducible Fermi surface, with the number of components equal to the number of layers. All potentials are electric; we do not treat magnetic potentials in this work. We include in this summary the bilayer quantum graphs studied in [60], which we call type 0.

Type-0 bilayer graphs. ([60])

1. The two layers are identical, and otherwise there is no restriction on the individual layers.
2. The layers are coupled by single edges connecting corresponding vertices.
3. The potentials on all connecting edges possess the same spectral asymmetry function $a(\lambda)$ mentioned above.

Type-1 multilayer graphs. (Fig. 1 left; and section 3)

1. Each layer is separable—it breaks into an infinite array of finite pieces when a vertex and its shifts are removed (Fig. 2).

2. The dispersion function $D(z, \lambda)$ of each layer is a polynomial function of a single function $\zeta(z, \lambda)$; for example, all layers may all have the same dispersion function.
3. Several layers are connected at the vertices of separation by edges or by a more complicated graph.
4. An example is AB-stacked graphene, with arbitrary potentials on the three edges of a period of each layer. Layers may be rotated 180°. See section 5.4.

The proof of Theorem 7 on type 1 employs a calculus for obtaining the dispersion function of a periodic graph in terms of the dispersion functions of component graphs, where the component graphs are joined at the periodic shifts of a single vertex (Lemma 5). It is a sort of periodic-graph version of surgery techniques for compact graphs, studied in [11].

Type-2 multilayer graphs. (Fig. 1 right; and section 4)

1. Each layer has the same underlying graph, which is bipartite with one vertex of each type, or color, per period (each edge connects vertices of different colors).
2. The potentials on corresponding edges in different layers are isospectral in the Dirichlet sense.
3. Several layers are connected along vertices of the same color by edges or more complicated graphs.
4. An example is AA-stacked graphene, with arbitrary potentials on the three edges of a period. Layers may be rotated 180°. See section 5.3.

The proof of Theorem 10 on type 2 is linear-algebraic. It is a generalization of AA-stacked bilayer graphene discussed in [60, §6], where it was noticed that the potentials of the connecting edges, miraculously, did not have to lie in the same asymmetry class in order to obtain reducibility of the Fermi surface.

Multi-layer graphene models. (Section 5)

A salient application of the theory we develop is to two-dimensional periodic graphs with hexagonal, or honeycomb, structure. Graphene is the most familiar of these structures. We will use the word "graphene" to encompass any periodic quantum graph with the hexagonal structure of graphene, shown in Fig. 4.

Quantum graphs offer an intermediate model between full partial differential equation models and tight-binding ones, and they have been used to model graphene and other honeycomb structures in single-layer form [18, 38, 4] and multi-layer form [19, 20, 21]. The model is also called a quantum or free-electron network model [18]; see [43, Appendix A] for a historical discussion.

The quantum-graph model of single-layer graphene satisfies the properties of the individual layers of both type 1 and type 2: (a) Being bipartite, each layer is separable at any vertex; and (b) isospectrality of the potentials on corresponding edges across layers implies that each layer is a polynomial in a common function $\zeta(z, \lambda)$. By applying the techniques of both types, one finds that very generally stacked multi-layer graphene has reducible Fermi surface. This includes AA-, AB-, ABC-, and mixed stacking, as illustrated in the figures of Section 5.

The differences between single- and multiple-layer graphene are expounded in [16, 1], which offers much physical context. The most important feature of two or more layers, which occurs typically but not always, is a transition from conical singularities of the dispersion relation (linear band structure at Dirac points) for a single layer to nonconical singularities (quadratic band structure) for multiple layers, accompanied by spectral gaps; see [51, 47, 15], for example. Refs. [33, 53, 56]

present some interesting work on opening gaps by twisting two layers relative to one another. The work [54] provides a review of physical phenomena of stacked bi-layer graphene.

The present work contributes to the spectral properties of graph models of multi-layer graphene with electric potentials in these ways: (1) The reducibility of the Fermi surface allows the construction of local defects in multi-layer graphene that would allow bound states within the radiation continuum (cf. [40]); (2) The theorems demonstrate the range of allowed potentials on the layers and the connecting edges in order to obtain a reducible Fermi surface, and (3) The theory offers insight into the effect of multiple layers on conical singularities, or Dirac cones. Particularly, a condition for conical singularities to persist in AA-stacked graphene is given (section 5.7, Proposition 11); this result is subsumed by [10, Theorem 2.4], which exploits symmetries to obtain Dirac cones; here it arises through different calculations.

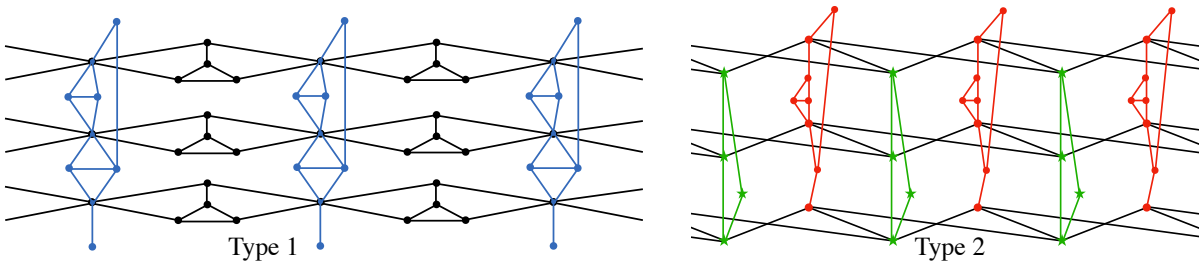

Figure 1: 1-periodic examples of multi-layer graphs with reducible Fermi surface. Type 1 (left): Each layer is a separable periodic graph whose dispersion function is a polynomial in a fixed Laurent polynomial $\zeta(z, \lambda)$. The layers are connected at corresponding vertices of separation by the periodic translates of a finite (blue) graph. Type 2 (right): Each layer has the same underlying bipartite periodic graph with two vertices per period, and the potentials on corresponding (vertically displaced) edges have the same Dirichlet spectrum. Vertically displaced green vertices are connected by periodic translates of a finite (green) graph; and similarly for the red vertices.

Quantum graphs have been used as models for a variety of physical systems, such as single- and multi-layer graphene, as mentioned above, tubes of graphene or other planar materials [35, 34, 38, 50, 61], and related band-gap structures [55, 43, 3, 22, 9]. We also refer the reader to the works [2, 36], the collection [24], and the monograph [12].

The multi-layer graphs types 0, 1, and 2, described above allow general vertex conditions of Robin type, defined below (see 2.1). The condition stipulates that the value of a function at a vertex v is proportional to a flux from the vertex into the adjacent edges, and the proportionality constant is called the Robin parameter α_v. Different values of α can model different types of atoms at the vertices. The Robin condition is essentially a δ-potential of strength α_v concentrated at a vertex v [26, Eq. 2.6], and it is also known as the δ vertex condition. A quantum graph with the Robin vertex condition emerges as the limit of a Schrödinger operator on a thickened graph, as the thickness tends to zero [26, §2–3]. Taking the limit in different ways results in other types of self-adjoint vertex conditions; see also [25, 17] for discussions of these limits and their physical relevance.

The Robin condition also allows different coupling strengths imparted by the edges (denoted by ε_e in (2.1) below). This accommodates, for example, adjusting interlayer couplings, which can be much weaker than the intralayer bonds [42, 48, 45, 5], and quite complex variations of atom interactions [14, 51]. This strength parameter has been implemented in the quantum-graph models of multi-layer graphene in [19, 20, 21].

Bound states in the continuum are impossible for locally defective periodic Schrödinger partial

differential operators in $\mathbb{R}^d$ [39, 37], and this makes the prospect of creating multi-layer structures where local defects can engender embedded eigenvalues intriguing. In Section 7, we show how to construct a local defect in a periodic quantum graph with reducible Fermi surface, that creates a bound state at an energy embedded in the continuous spectrum. We do this for AA- and AB-stacked bilayer graphene. The associated eigenstates are not those of compact support that are peculiar to graph operators, but rather, they decay exponentially with unbounded support. Bound states in the continuum are associated with interesting and useful resonance phenomena, with applications notably in optics—see for example [28, 27, 62, 32] and other references therein; and in the theory of Fano resonance—see the work of Fano [29] and a description of how it fits into the context of embedded eigenvalues in [58, Section 5.1]. A motivation for the present work is to understand the mechanisms underlying the creation of embedded eigenvalues and resonances in diverse material structures.

2 Periodic quantum graphs, Fermi surface, reducibility

This section lays down the notation for periodic quantum graphs and the Fermi surface. Lemma 5 introduces a calculus for joining two periodic graphs by the "single-vertex join", defined in Definition 4; this calculus serves as the basic tool for proving reducibility of multi-layer graphs of type 1.

2.1 Quantum graphs and notation

We give a brief account of periodic quantum graphs that is sufficient for the analysis in this paper. The notation specific to periodic graphs essentially follows [60, §3.1-3.2]; and the standard text [12] provides a more general exposition of quantum graphs.

The structure of a quantum graph begins with an underlying graph Γ, with vertex set $\mathcal{V}(\Gamma)$ and edge set $\mathcal{E}(\Gamma)$, and Γ becomes a metric graph when each edge e is coordinatized by an interval $[0, L_e]$. When referring to an edge e connecting vertices v and w, we write $e\{v, w\}$ when the edge is unoriented and $e(v, w)$ when the edge is oriented from v to w. A periodic graph has a free shift action of $\mathbb{Z}^d$, denoted by $x \mapsto gx$ for $x \in \Gamma$ and $g = (g_1, \ldots, g_d) \in \mathbb{Z}^d$. We assume that a fundamental domain of the action (a period of the graph) has finitely many vertices and edges. Then, each edge e is endowed with a Schrödinger operator

$$-\frac{d^2}{dx^2} + q_e(x) \qquad (0 < x < L_e).$$

A global operator on Γ is determined by coupling these edge operators by a condition at each vertex v. To define the coupling condition, each vertex v is endowed with a real weight α_v and each edge e is endowed with a real weight ε_e. Then, for a continuous function f on Γ (which has values on the vertices and along the edges), let f_e denote its restriction to the edge e. The vertex condition is

$$\sum_{e \in \mathcal{E}(v)} \varepsilon_e \, f_e'(v) \;=\; \alpha_v f(v), \tag{2.1}$$

which is called the Kirchoff or Neumann condition when $\alpha_v = 0$. The sum is over all edges incident to v, and the prime denotes the inward derivative, in the direction from the vertex into the edge. Thus, if an edge $e\{v, w\}$ is coordinatized by $x \in [0, L_e]$ running from v to w, then $f_e'(v) = df_e/dx(0)$ and $f_e'(w) = -df_e/dx(L_e)$.

The vertex condition (2.1) is called a Robin condition. The weight α_v, called a Robin coefficient, can be considered as a singular δ-potential of strength α_v at the vertex (see [26, Eq. 2.6] for example), and thus the condition is also called the δ vertex condition. The weight ε_e for an edge $e\{v, w\}$ controls the strength of the connection between vertices v and w. In multi-layer graphene, the inter-layer coupling is considered to be much weaker than the intra-layer bonds, and this is modeled by small values of ε_e on those edges that connect vertices in different layers.

These ingredients are sufficient to determine a self-adjoint operator A in the complex Hilbert space $L^2(\Gamma, \varepsilon)$ of weighted square-integrable functions on Γ, that is, functions f such that the following norm is finite:

$$\|f\|_{L^2(\Gamma,\varepsilon)} = \sum_{e\in\mathcal{E}(\Gamma)} \int_e \varepsilon_e |f(x)|^2 dx\,. \tag{2.2}$$

The operator A, being unbounded, has domain $\mathcal{D}(A)$ that is not all of $L^2(\Gamma, \varepsilon)$ but consists of those functions in $L^2(\Gamma, \varepsilon)$ whose restriction to each edge e is in the Sobolev space $H^2(e)$ and that are continuous on Γ and satisfy the Robin condition at each vertex. The pair (Γ, A) is called a quantum graph, and it is periodic provided that the coordinatizations of the edges, the potentials q_e, and the weights α_v and ε_e are invariant under the shift group $\mathbb{Z}^d$. All vertex conditions that correspond to self-adjoint operators in $L^2(\Gamma, \varepsilon)$ are described in [12, Theorem 1.4.4]. The operator A can in fact be applied to any continuous function on Γ that is in H^2 of each edge and satisfies the Robin vertex condition but that does not necessarily lie in $L^2(\Gamma, \varepsilon)$. The extended domain consisting of these functions will be called $\bar{\mathcal{D}}(A)$.

2.2 Spectral matrix and dispersion function

That A is a periodic operator is to say that it commutes with the $\mathbb{Z}^d$ action. According to the principles of harmonic analysis, one seeks simultaneous eigenfunctions u of A and the $\mathbb{Z}^d$ action,

$$Au = \lambda u \tag{2.3}$$

$$u(gx) = z^g u(x), \tag{2.4}$$

in which λ is the energy (eigenvalue of A) and $z = (z_1, \ldots, z_d) = (e^{ik_1}, \ldots, e^{ik_d})$ is the vector of Floquet multipliers (eigenvalues of the elementary shifts), with $z^g = \prod_{i=1}^d z_i^{g_i}$ for each $g = (g_1, \ldots, g_d) \in \mathbb{Z}^d$. Such u is called a Floquet (or Floquet-Bloch) mode of A. If the wavevector, or quasi-momentum, $k = (k_1, \ldots, k_d)$ is real, then u is a Bloch wave and the k_j are phase shifts of u across the d period vectors of the structure.

The pair (2.3, 2.4) is used to obtain a "spectral matrix" $\hat{A}(z, \lambda)$ for A, from which is derived the dispersion function and the Fermi surface. We now describe the elements of its derivation, which is described in more detail, including its relation to the Floquet-Bloch (Fourier) transform, in [60, §3.1-3.2].

Let us first consider the eigenvalue problem $Au = \lambda u$. Eigenfunctions u lie in $\bar{\mathcal{D}}(A)$ but not generally in $\mathcal{D}(A)$ since they are typically not square integrable. But if an eigenfunction does lie in $\mathcal{D}(A)$, then the energy λ is an eigenvalue of A considered as a self-adjoint operator in $L^2(\Gamma)$ and counts as point spectrum; and this only occurs for a discrete set of energies where A has a "flat band". These eigenfunctions are formed by linear combinations of compactly supported eigenfunctions. They are peculiar to graph operators (discrete and quantum; see [40]) and are discussed in Section 2.6.

The equation $Au = \lambda u$ means that u satisfies the ODE $-u'' + q_e(x)u = \lambda u$ on each edge. This allows one to use the Dirichlet-to-Neumann (DtN) map for this ODE on each edge to write the

equation $(A-\lambda)u=0$ solely in terms of the values of u on $\mathcal{V}(\Gamma)$. This leads to the reduction of $Au=\lambda u$ to a discrete graph problem, often called the discrete, or combinatorial, reduction of the quantum graph, which we now describe. By definition, the DtN map $N(\lambda)$ for an edge $e\{v,w\}$ takes the values of u at the vertices of the edge to the inward derivatives of u at the vertices, that is $N(\lambda)[u(v),u(w)]^t=[u'(v),u'(w)]^t$. The vertex condition (2.1) for u can then be written solely in terms of the values of u at the vertices. This results in a discrete, or combinatorial, reduction of the graph operator. To compute the DtN map for edge e, let e be parameterized by a variable $x\in[0,L]$ such that $x=0$ corresponds to v and $x=L$ corresponds to w. First, consider the transfer matrix (an entire function of λ)

$$T_e(\lambda) \;=\; \begin{bmatrix} c_e(\lambda) & s_e(\lambda) \\ c_e'(\lambda) & s_e'(\lambda) \end{bmatrix}, \tag{2.5}$$

which is defined by its action: It takes the value and x-derivative of u at vertex v to its value and x-derivative at w, that is, $T_e(\lambda)[u(0),du/dx(0)]^t=[u(L),du/dx(L)]^t$. The determinant of $T_e(\lambda)$ is always equal to 1. The DtN map is formed from the entries of $T_e(\lambda)$ by

$$N_e(\lambda) \;=\; \frac{1}{s_e(\lambda)} \begin{bmatrix} -c_e(\lambda) & 1 \\ 1 & -s_e'(\lambda) \end{bmatrix}. \tag{2.6}$$

Enforcing the second eigenvalue equation $u(gx)=z^g u(x)$ (2.4) allows one to restrict analysis of the solution to a single fundamental domain, or period, W. This is because this equation shows how the values $u(x)$ for $x\in W$ and the Floquet multipliers $z=(z_1,\ldots,z_d)$ determine the values of $u(gx)$ for $gx\in gW$ for any shift vector $g\in\mathbb{Z}^d$, just by multiplying by z^g. In this way, the equation $Au=\lambda u$ becomes equivalent to a discrete graph equation $\mathfrak{A}(\lambda)u=0$, where the function u is evaluated at the vertices only. (We will make use of $\mathfrak{A}(\lambda)$ only in section 7, where we construct embedded eigenvalues.)

Combining the analyses of both eigenvalue problems, the pair (2.3, 2.4) becomes equivalent to a homogeneous system of linear equations, depending on λ and z, for the values of u on the finite set of vertices in a fundamental domain. The square matrix for that system is what we call the spectral matrix $\hat{A}(z,\lambda)$,

$$\hat{A}(z,\lambda)u=0 \qquad \Longleftrightarrow \qquad u \text{ satisfies } (2.3, 2.4). \tag{2.7}$$

On the left, u is reused to denote the vector of values of the function u on the vertices.

The construction of $\hat{A}(z,\lambda)$ can be described algorithmically as follows. Let $\mathcal{V}_0$ and $\mathcal{E}_0$ denote the vertices and edges of a fixed fundamental domain W for (Γ,A). The matrix $\hat{A}(z,\lambda)$ is indexed by the vertices $\mathcal{V}_0$ minus those that have the Dirichlet condition. Given an edge $e\in\mathcal{E}_0$, there are vertices $v,w\in\mathcal{V}_0$ and $g\in\mathbb{Z}^d$ such that e connects v and gw. If both v and w have Robin conditions (including Neumann when the Robin parameter is 0) and $v\neq w$, then the following modified DtN matrix goes into the 2×2 submatrix of $\hat{A}(z,\lambda)$ indexed by v and w:

$$\tilde{N}_e(g,z,\lambda) \;=\; \frac{\varepsilon_e}{s_e(\lambda)} \begin{bmatrix} -c_e(\lambda) & z^g \\ z^{-g} & -s_e'(\lambda) \end{bmatrix}, \tag{2.8}$$

in which the off-diagonal entries come from the Floquet eigenvalue condition (2.4). If $v=w$, then $\varepsilon_e(z^g+z^{-g}-c_e(\lambda)-s_e'(\lambda))$ goes into the diagonal entry indexed by v. If w has the Dirichlet

condition, then $-\varepsilon_e c_e(\lambda)/s_e(\lambda)$ goes in the diagonal entry for v. Then a diagonal matrix with entries $-\alpha_v$ is added.

The dispersion function for (Γ, A) is defined by

$$D_{(\Gamma,A)}(z,\lambda) \;:=\; \det \hat{A}(z,\lambda), \tag{2.9}$$

and its zero set is the set of all (z,λ) pairs at which (Γ, A) admits a Floquet mode.

The spectral matrix does depend on the choice of fundamental domain, but of course the Floquet modes of (Γ, A) corresponding to null vectors of $\hat{A}(z,\lambda)$ are independent of this choice. More importantly, $\hat{A}(z,\lambda)$ and $D_{(\Gamma,A)}(z,\lambda)$ has poles in λ. Both are Laurent polynomials in z with coefficients that are meromorphic functions of λ. The poles lie at the roots of the functions $s(\lambda)$ for all edges. This set is denoted by

$$\sigma_D(\Gamma, A) \;=\; \{\lambda : \exists\, e \in \mathcal{E}(\Gamma),\, s_e(\lambda) = 0\}\,. \tag{2.10}$$

Observe that the function $s_e(\lambda)$ is independent of the orientation of the parameterization of e by $[0, L_e]$. We call $s_e(\lambda)$ the *Dirichlet spectral function* for e, as its roots are the Dirichlet eigenvalues of the operator $-d^2/dx^2 + q(x)$ on e.

This means that, with the construction of $\hat{A}(z,\lambda)$ as described, (2.7) is only valid for $\lambda \notin \sigma_D(\Gamma, A)$. This can be remedied by considering $\hat{A}(z,\lambda)$ and $D_{(\Gamma,A)}(z,\lambda)$ to be defined up to meromorphic factors in the following sense. For each λ, there is an equivalent quantum graph $(\dot{\Gamma}, \dot{A})$ such that $\lambda \notin \sigma_D(\dot{\Gamma}, \dot{A})$. This graph is obtained by inserting artificial vertices in the interior of edges of Γ, as described in [41, §IV], and imposing the Kirchhoff vertex condition at the new vertices so that the operator does not change. The following result is proved in section 8.

Proposition 1. *Let (Γ, A) be a periodic quantum graph, let $e\{v_1, v_2\}$ be an edge of Γ. Let $(\dot{\Gamma}, \dot{A})$ be the periodic quantum graph obtained by placing an additional vertex v in the interior of e (and gv in each shift ge), thus dividing e into two edges $e_1\{v_1, v\}$ and $e_2\{v, v_2\}$, with the potentials on e_1 and e_2 being inherited from q_e on e. Let $s(\lambda)$, $s_1(\lambda)$, and $s_2(\lambda)$ be the Dirichlet spectral functions for the edges e, e_1, and e_2. Then*

$$s_1(\lambda)s_2(\lambda)\, D_{(\dot{\Gamma},\dot{A})}(z,\lambda) \;=\; \pm s(\lambda)\, D_{(\Gamma,A)}(z,\lambda). \tag{2.11}$$

By inserting an extra vertex at an appropriate point in each edge that has λ as a Dirichlet eigenvalue, the spectral matrix and dispersion function become analytic at λ.

2.3 The Fermi surface

As described above, the zero-set of the dispersion function $D_{(\Gamma,A)}(z,\lambda)$ for (Γ, A) is the set of all (z,λ) pairs at which (Γ, A) admits a Floquet mode. This relation $D_{(\Gamma,A)}(z,\lambda) = 0$ in $(\mathbb{C}^*)^d \times \mathbb{C}$ is called the dispersion relation or the Bloch variety of the periodic operator A. By fixing an energy $\lambda \in \mathbb{C}$, one obtains the *Floquet surface*, or Floquet variety, of (Γ, A):

$$\Phi_\lambda = \Phi_{(\Gamma,A),\lambda} = \big\{z \in (\mathbb{C}^*)^d : D_{(\Gamma,A)}(z,\lambda) = 0\big\}. \tag{2.12}$$

When considered as a set of wavevectors $(k_1, \ldots, k_d) \in \mathbb{C}$ (with $z_j = e^{ik_j}$), it is the *Fermi surface* of (Γ, A). We will just call Φ_λ the "Fermi surface." The spectrum of (Γ, A) consists of all energies λ such that the Fermi surface intersects the d-torus $\mathbb{T}^d = \{z \in \mathbb{C}^d : |z_1| = \cdots = |z_d| = 1\}$,

$$\sigma_{(\Gamma,A)} = \Big\{\lambda \in \mathbb{C} : \Phi_{(\Gamma,A),\lambda} \cap \mathbb{T}^d \neq \emptyset\Big\}\,. \tag{2.13}$$

Importantly, when Γ is disconnected, with each connected component being a compact graph, a fundamental domain can be chosen to be one component Γ_0, and thus $\hat{A}(z,\lambda)$ and $D(z,\lambda)$ are independent of z. All of the matrices (2.8) have $g=0$ and reduce to the Dirichlet-to-Neumann maps for the edges. In this case, the spectral matrix, which can be denoted by $\hat{A}(\lambda)$, is the spectral matrix of A confined to the finite graph Γ_0, and the roots of its determinant $D(\lambda)$ are the eigenvalues of this finite quantum graph.

The Fermi surface is an algebraic set in $(\mathbb{C}^*)^d$, and it is ***reducible*** at λ whenever Φ_λ is the union of two algebraic sets. This occurs whenever $D(z,\lambda)$ is factorable into two polynomials, neither of which is a monomial. One should be aware of the situation when a Laurent polynomial $D_1(z,\lambda)^m$ divides $D(z,\lambda)$, with $m>1$, particularly when $D(z,\lambda) = D_1(z,\lambda)^m$. This makes Φ_λ reducible on account of having a component of multiplicity greater than 1.

2.4 A calculus for joining two periodic graphs

The lemma in this section is the building block for the analysis of the Fermi surfaces for multi-layer quantum graph operators of type 1. It can be viewed as a sort of periodic-graph version of the surgery principles for finite quantum graphs in [11]. These describe how the spectrum of a new graph is related to the spectra of old graphs under various modifications and joinings. When writing and manipulating formulas dealing with joining two quantum graphs together, it will be convenient to use the following abbreviated notation for the dispersion function of a periodic quantum graph (Γ, A), which emphasizes the dependence on Γ,

$$[\Gamma] := D_{(\Gamma,A)}(z,\lambda). \tag{2.14}$$

This notation will be used only in the rest of section 2 and in section 3, when A, z, and λ fall into the background and the vertices where the joining takes place become important.

Definition 2 (Γ^v)**.** *Let Γ be a d-periodic graph, and let v be a vertex of Γ of degree r. Denote by Γ^v the periodic graph obtained by replacing, for each $g\in\mathbb{Z}^d$, the vertex gv by r terminal vertices incident to the r edges that are incident to gv in Γ.*

If a Schrödinger operator A is defined on Γ as a metric graph, define a Schrödinger operator A^v on Γ^v as follows.

Definition 3 ((Γ^v, A^v))**.** *Let (Γ, A) be a d-periodic quantum graph containing vertex $v\in\mathcal{V}(\Gamma)$. Denote by (Γ^v, A^v) the quantum graph obtained by replacing the vertex condition at each vertex in the orbit $\{gv : g\in\mathbb{Z}^d\}$ in Γ with the Dirichlet condition. Thus Γ may as well be replaced by Γ^v.*

Definition 4 (Single-vertex join $\Gamma_1(v_1\,v_2)\Gamma_2$)**.** *Let Γ_1 and Γ_2 be d-periodic quantum graphs with Robin parameter α_1 at $v_1\in\mathcal{V}(\Gamma_1)$ and α_2 at $v_2\in\mathcal{V}(\Gamma_2)$. The* single-vertex join *of Γ_1 and Γ_2 at the pair (v_1,v_2), denoted by $\Gamma_1(v_1\,v_2)\Gamma_2$, is a quantum graph with vertex set $\mathcal{V}(\Gamma_1)\cup\mathcal{V}(\Gamma_2)/\equiv$, in which $gv_1\equiv gv_2$ for all $g\in\mathbb{Z}^d$ and edge set $\mathcal{E}(\Gamma_1)\cup\mathcal{E}(\Gamma_2)$. A Robin vertex condition with parameter $\alpha_1+\alpha_2$ is imposed at the joined vertices $gv_1\equiv gv_2$, and all other vertex conditions are inherited from Γ_1 and Γ_2. If the Robin parameter at the joined vertex $v_1\equiv v_2$ is changed to α, the resulting graph is denoted by $\Gamma_1(v_1\,v_2)_\alpha\,\Gamma_2$.*

Lemma 5. *Let Γ_1 and Γ_2 be d-periodic quantum graphs with $v_1\in\mathcal{V}(\Gamma_1)$ and $v_2\in\mathcal{V}(\Gamma_2)$. Then the dispersion function for $\Gamma_1(v_1,v_2)\Gamma_2$ is*

$$[\Gamma_1(v_1,v_2)\Gamma_2] \;=\; [\Gamma_1]\,[\Gamma_2^{v_2}] + [\Gamma_1^{v_1}]\,[\Gamma_2]\,, \tag{2.15}$$

and the dispersion function for $\Gamma_1(v_1\,v_2)_\alpha\,\Gamma_2$ *is*

$$[\Gamma_1(v_1\,v_2)_\alpha\,\Gamma_2] = [\Gamma_1]\,[\Gamma_2^{v_2}] + [\Gamma_1^{v_1}]\,[\Gamma_2] + (\alpha-\alpha_1-\alpha_2)\,[\Gamma_1^{v_1}]\,[\Gamma_2^{v_2}]\,. \tag{2.16}$$

Proof. Let A_1 and A_2 be the operators associated with the quantum graphs Γ_1 and Γ_2, and let $\hat{A}_1(z,\lambda)$ and $\hat{A}_2(z,\lambda)$ be the spectral matrices of these operators. Let $\hat{A}_1^0(z,\lambda)$ and $\hat{A}_2^0(z,E)$ be the spectral matrices of the operators associated with $\Gamma_1^{v_1}$ and $\Gamma_2^{v_2}$. By ordering the vertices of a fundamental domain of Γ_1 such that v_1 is listed last, and ordering the vertices of a fundamental domain of Γ_2 such that v_2 is listed first, one obtains the block decomposition

$$\hat{A}_1 = \begin{bmatrix} \hat{A}_1^0 & a_1 \\ a_1^* & a_1^0 \end{bmatrix}, \qquad \hat{A}_2 = \begin{bmatrix} a_2^0 & a_2^* \\ a_2 & \hat{A}_2^0 \end{bmatrix}, \tag{2.17}$$

in which a_1 and a_2 are column vectors and a_1^0 and a_2^0 are scalars.

The matrix $\hat{A}$ of the operator associated with $\Gamma_1(v_1\,v_2)\Gamma_2$ is

$$\hat{A} \;=\; \begin{bmatrix} \hat{A}_1^0 & a_1 & \mathbf{0} \\ a_1^* & a_1^0+a_2^0 & a_2^* \\ \mathbf{0} & a_2 & \hat{A}_2^0 \end{bmatrix}. \tag{2.18}$$

Notice that the entry $a_1^0+a_2^0$ incorporates the Robin parameter $\alpha_1+\alpha_2$. The first statement of the theorem is just the following statement about determinants:

$$\det(\hat{A}) \;=\; \det(\hat{A}_1)\det(\hat{A}_2^0) + \det(\hat{A}_1^0)\det(\hat{A}_2).$$

The matrix Floquet transform for $\Gamma_1(v_1\,v_2)_\alpha\,\Gamma_2$ is obtained by adding $\alpha-\alpha_1-\alpha_2$ to the term $a_1^0+a_2^0$ in (2.18), and the second statement of the theorem follows. □

2.5 Separable periodic graphs

The class of multi-layer graphs we call type 1 is built on separable layers. Each layer has the property that, when severed periodically at a certain vertex, it falls apart into a d-dimensional array of identical finite graphs, as illustrated in Fig. 2. This is made precise as follows.

Definition 6 (separable periodic graph)**.** *A d-periodic graph Γ is* separable at $v\in\mathcal{V}(\Gamma)$ *if Γ^v is the union of the $\mathbb{Z}^d$ translates of a finite graph, or, equivalently, if Γ^v has compact connected components.*

2.6 Flat bands

We include a remark about "flat bands" of periodic graph operators. A flat band is a component of the dispersion relation of the form $\lambda=\lambda_0$, where λ_0 is a fixed energy. Such a band arises when the dispersion function has a z-independent meromorphic factor $m(\lambda)$, say $D(z,\lambda)=m(\lambda)\tilde{D}(z,\lambda)$. The values of λ_0 are the roots of $m(\lambda)$. This means that there is a Floquet mode at energy λ_0 for each $z\in(\mathbb{C}^*)^d$, or equivalently for each quasimomentum $(k_1,\dots,k_d)$. When considering components of the Fermi surface Φ_λ at a given energy λ, we are concerned with reducibility of $\tilde{D}(z;\lambda)$ into two or more Laurent polynomials in z that are not constant functions of z, and therefore we will not concern ourselves with flat bands in subsequent sections.

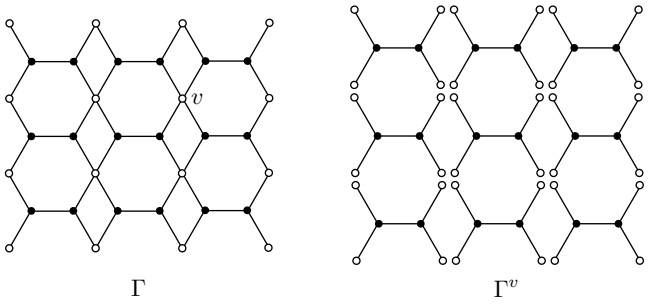

Figure 2: A 2-periodic graph that is separable at a vertex v; and the corresponding separated graph Γ^v.

The energy of a flat band is an eigenvalue of infinite multiplicity for the periodic operator, meaning that it has an eigenspace in $L^2(\Gamma)$ of infinite dimension [23, 38]. In the case of single-layer graphene with the same potential on each edge, the flat bands occur exactly at the Dirichlet eigenvalues associated with an edge, and each eigenfunction is a linear combination of "loop states" supported on a hexagon [38]. These loop states vanish at all vertices. Because of this, all these eigenfunctions, and therefore the flat bands, persist when several layers are stacked according the two constructions described in this work. More generally, flat bands of any single layer persist in a multi-layer graph whenever eigenfunctions of the layer vanish on the vertices involved in the coupling to other layers. The eigenfunctions of flat bands of periodic quantum graphs can in general be nonzero at vertices.

3 Type 1: Multi-layer graphs with separable layers

This section develops a class of multi-layer graphs whose individual layers are separable and whose Fermi surface is reducible, with several components. A 1-periodic illustration is in Fig. 1(left). An example is AB-stacked graphene, which is discussed in Section 5.4.

3.1 Type-1 multi-layer graphs

First, we define the *layers* (black in Fig. 1(left)) and the *connector graph* (blue in Fig. 1(left)). Let $\zeta(z,\lambda)$ be a Laurent polynomial in $z = (z_1, \dots, z_d)$ with coefficients that are meromorphic in λ. The j-th layer ($j = 1, \dots, n$) is a d-periodic quantum graph (Λ_j, A_j), with a distinguished vertex v_j and such that the dispersion function $d_j(z,\lambda)$ of (Λ_j, A_j) and the dispersion function $\mathring{d}_j(z,\lambda)$ of $(\Lambda_j^{v_j}, A_j^{v_j})$ are polynomial functions of $\zeta(z,\lambda)$ with coefficients that are meromorphic in λ,

$$d_j(z,\lambda) \;=\; p_j\big(\zeta(z,\lambda),\lambda\big), \tag{3.19}$$

$$\mathring{d}_j(z,\lambda) \;=\; \mathring{p}_j\big(\zeta(z,\lambda),\lambda\big). \tag{3.20}$$

Of course, we have in mind specifically the situation in which each layer Λ_j is separable at v_j. This is because, in this case, $\Lambda_j^{v_j}$ is a disjoint union of compact graphs, and thus its dispersion function is a meromorphic function $f_j(\lambda)$ and therefore a degree-0 polyomial in $\zeta(z,\lambda)$,

$$\mathring{d}_j(z,\lambda) \;=\; f_j(\lambda). \tag{3.21}$$

It will be useful to allow $\mathring{p}_j$ to be a more general polynomial in applications such as ABC-stacked graphene in Section 5. The connector graph is a finite quantum graph (Σ, B), together with a list of distinct vertices $w_j \in \mathcal{V}(\Sigma)$ ($j = 1, \dots, n$).

From these ingredients, an n-layer quantum graph (Γ, A) of type 1, as illustrated on the left of Fig. 1, is formed as follows. The vertex v_j is merged, or identified, with w_j. In like manner, for each $g \in \mathbb{Z}^d$, the translated vertices $gv_1, \ldots, gv_n$ are coupled by another copy of Σ, called $g\Sigma$. The resulting periodic graph Γ is what we call a type-1 multi-layer graph. Its edge set consists of the edges of each layer Λ_j and the edges of each translate $g\Sigma$ of Σ. By denoting the identification of merged vertices by the equivalence relation $\equiv$, the vertex and edge sets of Γ are

$$\mathcal{V}(\Gamma) \;=\; \left(\bigcup_{j=1}^{n} \mathcal{V}(\Lambda_j) \;\cup\; \bigcup_{g\in\mathbb{Z}^d} \mathcal{V}(g\Sigma) \right) / \equiv \tag{3.22}$$

$$\mathcal{E}(\Gamma) \;=\; \bigcup_{j=1}^{n} \mathcal{E}(\Lambda_j) \;\cup\; \bigcup_{g\in\mathbb{Z}^d} \mathcal{E}(g\Sigma). \tag{3.23}$$

The Schrödinger operator A on Γ has the same differential-operator expression as the operators A_j and B on the elemental graphs Λ_j and Σ, and the Robin parameter of an equivalence class of merged vertices (now a single vertex of Γ) is assigned the sum of the Robin parameters of all the vertices that were merged.

Observe that it is possible to allow several of the vertices w_j to be equal. In this case, one might as well merge all the layers that are attached to that vertex into a single layer according to the single-vertex join in Definition 4, applied several times. According to the calculus of Lemma 5, the degree of the polynomial p_j for this new layer is the maximum of the degrees of the polynomials of the joined components.

Theorem 7. *Let (Γ, A) be an n-layer d-periodic quantum graph of type 1. Its dispersion function $D(z,\lambda)$ is a polynomial in $\zeta(z,\lambda)$ with coefficients that are meromorphic functions of λ,*

$$D(z,\lambda) \;=\; P(\zeta(z,\lambda),\lambda), \tag{3.24}$$

and the degree of P as a polynomial in ζ is

$$\deg P \;=\; \sum_{j=1}^{n} \deg p_j. \tag{3.25}$$

The proof applies Lemma 5 iteratively as successive layers are connected through the connector graph.

Proof. When the number of layers is zero, (Γ, A) is the union $\cup_{g\in\mathbb{Z}^d} g\Sigma$ of disconnected finite components with the operator B acting on each component. The dispersion function is a meromorphic function of λ, independent of z, and is thus trivially a polynomial in $\zeta(z,\lambda)$ of degree 0, with coefficients that are meromorphic in λ. As the induction hypothesis, let the theorem hold with n replaced by $n-1$, with $n \geq 1$.

Let (Γ, A) be the type-1 n-layer quantum graph supposed in the theorem, with layers (Λ_j, A_j) separable at v_j $(1 \leq j \leq n)$ and connector graph (Σ, B) with distinct joining vertices $\{w_j\}_{j=1}^n$. If any of the polynomials p_j has degree 0, then Λ_j is a disjoint union of $\mathbb{Z}^d$ translates of a finite graph, and this finite graph might as well be joined with the connector graph Σ. Therefore, we assume that each $\deg p_j \geq 1$ for all $j : 1 \leq j \leq n$.

Denote by $(\tilde{\Gamma}, \tilde{A})$ the type-1 $(n-1)$-layer quantum graph built from the layers $\{(\Lambda_j, A_j)\}_{j=1}^{n-1}$ and the connector objects (Σ, B) and $\{w_j\}_{j=1}^{n-1}$. Note that $(\tilde{\Gamma}^{w_n}, \tilde{A}^{w_n})$ is the type-1 $(n-1)$-layer

quantum graph built from the layers $\{(\Lambda_j, A_j)\}_{j=1}^{n-1}$ and the connector objects (Σ^{w_n}, B^{w_n}) and $\{w_j\}_{j=1}^{n-1}$. Denote by $\tilde{D}(z,\lambda)$ and $\tilde{D}^0(z,\lambda)$ the dispersion functions of $(\tilde{\Gamma}, \tilde{A})$ and $(\tilde{\Gamma}^{w_n}, \tilde{A}^{w_n})$. By the induction hypothesis, they are polynomials in $\zeta(z,\lambda)$ with coefficients that are meromorphic in λ, and both are of degree $\sum_{j=1}^{n-1} \deg p_j$.

The graph (Γ, A) is the single-vertex join of $(\tilde{\Gamma}, \tilde{A})$ and Λ_n,

$$\Gamma \;=\; \tilde{\Gamma}(w_n, v_n)\Lambda_n \tag{3.26}$$

and the calculus of Lemma 5 yields

$$[\Gamma] \;=\; [\tilde{\Gamma}][\Lambda_n^{v_n}] + [\tilde{\Gamma}^{w_n}][\Lambda_n]. \tag{3.27}$$

Since Λ_n is separable at v_n, $[\Lambda_n^{v_n}]$ is independent of z, so the degree of the first term on the right-hand side of (3.27), as a polynomial in ζ, is $m = \sum_{j=1}^{n-1} \deg p_j$. The degree of the second term as a polynomial in ζ is $m + \deg p_n$. This completes the induction. □

A special case of this theorem occurs when there is only one layer. The connector graph Σ is then viewed as a periodic "decoration" of Λ_1. The result is the following corollary. Much more is known about decorated periodic graphs, particularly with regard to opening spectral gaps [57].

Corollary 8 (Decorated graphs)**.** *Let (Γ, A) be a d-periodic quantum graph that is separable at vertex v, and let (Σ, B) be a finite decorator graph with distinguished vertex $w \in \mathcal{V}(\Sigma)$. Let $\ell(\lambda)$ denote the spectral function of (Γ^v, A^v), and let $h(\lambda)$ and $h^0(\lambda)$ denote the spectral functions of (Σ, B) and (Σ^w, B^w).*

Denote by $(\bar{\Gamma}, \bar{A})$ the "decorated graph" obtained by the single-vertex join of (Γ, A) and $\Delta = \cup_{g\in\mathbb{Z}^d} g\Sigma$ at the vertices v and w. If the Fermi surface of (Γ, A) at energy λ is given by

$$D(z,\lambda) \;=\; 0, \tag{3.28}$$

then the Fermi surface of $(\bar{\Gamma}, \bar{A})$ at λ is given by

$$D(z,\lambda) \;=\; -\frac{\ell(\lambda)h(\lambda)}{h^0(\lambda)}. \tag{3.29}$$

Proof. Actually, this is a bit more than just a corollary to the theorem. The theorem says that $[\bar{\Gamma}]$ is a function of $D(\lambda, z)$ that is linear in $D(z,\lambda)$ (take $\zeta(z,\lambda) = D(z,\lambda)$). But we can find the coefficients from Lemma 5, which says $[\bar{\Gamma}] \;=\; [\Gamma][\Delta^w] + [\Gamma^v][\Delta]$, or

$$[\bar{\Gamma}] \;=\; D(z,\lambda)h^0(\lambda) + \ell(\lambda)h(\lambda). \tag{3.30}$$

The Fermi surface of $(\bar{\Gamma}, \bar{A})$ is $[\bar{\Gamma}] = 0$, from which follows the result. □

The polynomial $P(\zeta,\lambda)$ in Theorem 7 factors into $m = \sum_{j=1}^{n} \deg p_j$ linear factors as a function of ζ, and each factor corresponds to a component of the Fermi surface of (Γ, A). Thus the following theorem is an immediate consequence of Theorem 7, and parses the result in terms of components of the Fermi surface.

Theorem 9. *The Fermi surface of a type-1 n-layer d-periodic quantum graph is reducible into $m = \sum_{j=1}^{n} \deg p_j$ components (with possible multiplicities). Each component is of the form*

$$\zeta(z,\lambda) \;=\; \mu(\lambda). \tag{3.31}$$

For each λ, the m (not necessarily distinct) values of $\mu(\lambda)$ are the roots of $P(\zeta,\lambda)$.

3.2 Coupling several type-1 multi-layer graphs

Multi-layer graphs themselves can be used as the layers of more complex multi-layer graphs. This ideas will be used for ABC-stacked graphene in section 5.5. Observe that single-layer graphene is separable at each of the two vertices of a fundamental domain.

Let (Γ_j, A_j) be d-periodic type-1 multi-layer graphs based on separable layers described in the previous section, with a common composite Floquet variable $\zeta(z,\lambda)$. Suppose that each (Γ_j, A_j) has a distinguished layer (Λ_j, B_j) such that Λ_j is separable at a vertex v_j other than the one used in constructing (Γ_j, A_j). The dispersion function of $(\Lambda_j^{v_j}, B_j^{v_j})$ is therefore independent of z and can be used as a layer in a type-1 multi-layer graph. By replacing the layer (Λ_j, B_j) in the construction of (Γ_j, A_j) by the layer $(\Lambda_j^{v_j}, B_j^{v_j})$, one obtains $(\Gamma_j^{v_j}, A_j^{v_j})$. The point here is that, by Theorem 7, both (Γ_j, A_j) and $(\Gamma_j^{v_j}, A_j^{v_j})$ have dispersion function that is a polynomial in $\zeta(z,\lambda)$. The theorem is then applied again with (Γ_j, A_j) as the layers, which are coupled by an arbitrary finite connector graph (Σ, C) by joining the vertices v_j with given vertices w_j of Σ.

4 Type 2: Multi-layer graphs with bipartite layers

This section generalizes the construction in [60, §6] from bi-layer to n-layer quantum graphs and from single-edge coupling to coupling by general graphs, as illustrated on the right in Fig. 1. Each layer has the same underlying graph, which is bipartite with exactly one "red" and one "green" vertex in a fundamental domain. The layers are connected by one graph connecting the n red vertices in a fundamental domain and another graph connecting the n green vertices in a fundamental domain. A topical example is AA-stacked graphene, which is discussed in Section 5.3.

4.1 Coupling by arbitrary finite graphs

Given that the quantum graph $(\Lambda, \mathring{A})$, for a given layer, has underlying graph Λ which is bipartite with one red and one green vertex per period, the Floquet transform of its discrete reduction is a 2×2 matrix

$$\hat{\mathring{A}}(z,\lambda) = \begin{bmatrix} b_1(\lambda) & w(z,\lambda) \\ w(z^{-1},\lambda) & b_2(\lambda) \end{bmatrix}, \tag{4.32}$$

in which $b_i(\lambda)$ are meromorphic functions of λ and $w(z,\lambda)$ is a Laurent polynomial in $z = (z_1, \dots, z_d)$ with coefficients that are meromorphic in λ. (See section 5.1 for the case of graphene.) Specifically, $w(z,\lambda)$ is a sum over some finite subset $Z \subset \mathbb{Z}^d$,

$$w(z,\lambda) \;=\; \sum_{\ell\in Z} \frac{\varepsilon_\ell\, z^\ell}{s_\ell(\lambda)}\,, \tag{4.33}$$

in which $s_\ell(\lambda)$ is the s-function for the potential $q(x)$ on the edge connecting a green vertex in a given fundamental domain with a red vertex in the domain shifted by $\ell \in \mathbb{Z}^d$, and $z^\ell = z_1^{\ell_1} \cdots z_n^{\ell_n}$ and ε_ℓ is the weight for that edge.

The requirement for the multi-layer graphs in the theorem below is that $w(z,\lambda)$ be identical over all the layers; but the functions $b_1(\lambda)$ and $b_2(\lambda)$ are allowed to vary from layer to layer. This means that each layer must have the same underlying graph Λ, and that for any given edge of Λ, the potential at each layer must have the same $s(\lambda)$-function, or, equivalently, the potentials must have the same Dirichlet spectrum. Indeed, the Dirichlet spectrum of $-d^2/dx^2 + q(x)$ on an interval and the function $s(\lambda)$ determine each other; see [52, Ch. 2 Theorem 5], for example.

Several such graphs (Λ, A_k), $k = 1, \ldots, n$, with the same $w(z, \lambda)$, are coupled to form an n-layer quantum graph (Γ, A) as depicted on the right in Fig. 1. Start with the disjoint union of the n graphs (Λ, A_k). Then replace the n red vertices in a fundamental domain with a finite quantum graph (Σ_1, B_1) whose vertex set includes those n red vertices plus (possibly) additional ones. Another finite graph (Σ_2, B_2) connects the green vertices together. These two coupling graphs are repeated periodically. The simplest case is when two successive single layers (Λ, A_k) and (Λ, A_{k+1}) are connected with a single edge between corresponding red vertices and a single edge between corresponding green vertices. The spectral matrix for (Γ, A) is

$$\begin{aligned} \hat{A}(z,\lambda) &= \begin{bmatrix} \mathbf{b}_1(\lambda) & w(z,\lambda)Q \\ w(z^{-1},\lambda)Q^T & \mathbf{b}_2(\lambda) \end{bmatrix} + \begin{bmatrix} B_1(\lambda) & 0 \\ 0 & B_2(\lambda) \end{bmatrix} \\ &= \begin{bmatrix} \tilde{B}_1(\lambda) & w(z,\lambda)Q \\ w(z^{-1},\lambda)Q^T & \tilde{B}_2(\lambda) \end{bmatrix}, \end{aligned} \tag{4.34}$$

in which Q is the $m_1 \times m_2$ matrix with the $n \times n$ identity matrix in its upper left, all other entries being zero; $\mathbf{b}_1(\lambda)$ (*resp.* $\mathbf{b}_2(\lambda)$) is a square diagonal matrix of size $n+m_1$ (*resp.* $n+m_2$),

$$\mathbf{b}_1(\lambda) = \operatorname*{diag}_{j=1\ldots n} b_1^j(\lambda) \oplus 0_{m_1} = \begin{bmatrix} b_1^1(\lambda) & & & & & \\ & \ddots & & & & \\ & & b_1^n(\lambda) & & & \\ & & & 0 & & \\ & & & & \ddots & \\ & & & & & 0 \end{bmatrix}; \tag{4.35}$$

$B_1(\lambda)$ is the $m_1 \times m_1$ spectral matrix of the coupling graph for the red vertices and the $m_2 \times m_2$ matrix $B_2(\lambda)$ is for the green vertices; and $\tilde{B}_j(\lambda) = \mathbf{b}_j(\lambda) + B_j(\lambda)$.

The dispersion function of (Γ, A) is

$$D(z,\lambda) = \det \hat{A}(z,\lambda) = \det\big(\tilde{B}_1(\lambda)\big) \det\Big(\tilde{B}_2(\lambda) - w(z,\lambda)w(z^{-1},\lambda)\, Q^T \tilde{B}_1(\lambda)^{-1} Q\Big) \tag{4.36}$$

$$= P\big(w(z,\lambda)w(z^{-1},\lambda), \lambda\big), \tag{4.37}$$

in which $P(\cdot, \lambda)$ is a polynomial of degree n with coefficients that are meromorphic functions of λ. For a single layer, this polynomial is just a linear function of the composite Floquet variable

$$\zeta(z,\lambda) := w(z,\lambda)w(z^{-1},\lambda). \tag{4.38}$$

We have proved the following theorem.

Theorem 10 (bipartite layers)**.** *Let (Γ, A) be a multi-layer periodic quantum graph obtained by coupling n quantum graphs (Λ, A_k), $k = 1, \ldots, n$, in which the underlying graph Λ is bipartite with exactly one vertex of each "color" in a fundamental domain; and on corresponding edges, the weights are identical and the potentials defining the operators A_k have the same Dirichlet spectrum; and the coupling is effectuated by finite graphs of each color, as described for a type-2 multi-layer graph. The Robin parameters may be different across layers.*

For each energy λ, the Fermi surface of (Γ, A) has n components (which may have multiplicity greater than 1). The components are of the form

$$\zeta(z,\lambda) = \rho(\lambda), \tag{4.39}$$

in which $\rho(\lambda)$ is a root of the polynomial (4.36). The multiplicity of a component is equal to the multiplicity of the corresponding root.

The isospectral sets of L^2 potentials $q(x)$ on an interval are well understood; each isospectral set is parameterized by the set of sequences of certain spectral data, as described in [52].

4.2 Stacking by edges

When n successive layers are connected by edges (or decorated edges), the matrix Q in expression (4.36) becomes the $n\times n$ identity matrix I_n, and the dispersion function simplifies to

$$D(z,\lambda) \;=\; \det\big(\tilde{B}_1(\lambda)\tilde{B}_2(\lambda) - \zeta(z,\lambda)I_n\big), \tag{4.40}$$

and therefore the components of the Fermi surface are

$$\zeta(z,\lambda) \;=\; \rho_j(\lambda), \quad j = 1,\ldots,n, \tag{4.41}$$

where ρ_j are the eigenvalues of the matrix $\tilde{B}_1(\lambda)\tilde{B}_2(\lambda)$.

As the connector graphs are linear graphs, their spectral matrices $B_i(\lambda)$ are tridiagonal, with DtN matrices for the connector edges along the principal 2×2 submatrices.

Remark on decorated edges. For the sake of completeness, we mention that the edges in any of the quantum graphs we consider may as well be "decorated edges", as illustrated in Fig. 3 for a single-layer graphene structure. A decorated edge is a finite graph that has two distinguished terminal vertices that act as the two vertices of the decorated edge. Particularly, in a type-2 multi-layer graph, the single layers, even when decorated, can essentially still be considered as being bipartite. Allowing decorations on an edge can be thought of loosely as allowing a broader class of potentials on the edge. A decorated edge admits a Dirichlet-to-Neumann map that straightforwardly generalizes that of an edge. When forming the spectral matrix $\hat{A}(z,\lambda)$, this DtN map is used, as described in section 2.2, and only the two terminal endpoints of the decorated edge enter into the vertex set that indexes the matrix.

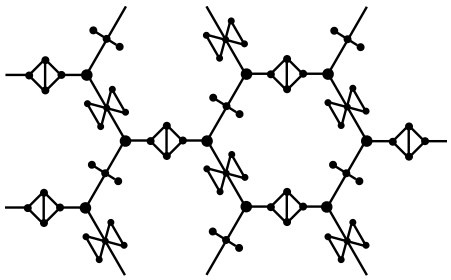

Figure 3: Quantum-graph graphene model with decorated edges.

5 Multi-layer graphene

We apply the theory developed in this work to quantum-graph models of multi-layer graphene structures. Very general stacking of graphene, where the layers are shifted or rotated, results in a reducible Fermi surface. We also discuss the conical singularities at wavevectors $(k_1,k_2) = \pm(2\pi/3, -2\pi/3)$ for single-layer graphene and how stacking multiple layers destroys them.

5.1 The single layer

A graph model of graphene is hexagonal and bipartite, having two vertices and three edges of length 1 per fundamental domain. Being bipartite, it is also separable at any vertex (see, for example, [38]).

The most general quantum-graph model $(\mathring{\Lambda}, \mathring{A})$ for which the differential operator on the edges is of the form $-d^2/dx^2 + q(x)$ features three potentials, one for each edge in a period, and two Robin parameters α_i, one for each vertex v_i $(i = 1, 2)$ in a period. The potentials will be denoted by $q_i(x)$ $(i = 0, 1, 2)$ as in Fig. 4 and the corresponding transfer matrices by

$$T_i(\lambda) \;=\; \begin{bmatrix} c_i(\lambda) & s_i(\lambda) \\ c_i'(\lambda) & s_i'(\lambda) \end{bmatrix} \qquad (i = 0, 1, 2). \tag{5.42}$$

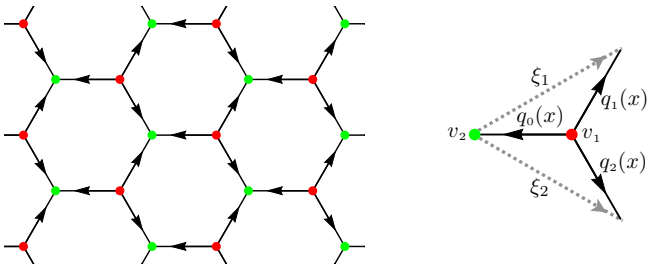

Figure 4: Single-layer graphene $\mathring{\Gamma}$ and its fundamental domain. The arrows on the edges indicate the direction of the x-interval $[0, 1]$ in the parameterization of the edges. The vectors ξ_1 and ξ_2 generate the periodic shifts.

Let ξ_1 and ξ_2, as illustrated in Fig. 4, be generators of the periodicity in the sense that the action of $(n_1, n_2) \in \mathbb{Z}^2$ on $\mathring{\Gamma}$ shifts the graph along the vector $n_1\xi_1 + n_2\xi_2$ in the plane so that it falls exactly into itself. The components of the vector (z_1, z_2), the Floquet multipliers, are the eigenvalues of the shifts by ξ_1 and ξ_2 corresponding to a Floquet mode. The spectral matrix (4.34) of this quantum graph at energy λ is

$$\mathring{\hat{A}}(z_1, z_2, \lambda) \;=\; \begin{bmatrix} b_1(\lambda) & w(z, \lambda) \\ w(z^{-1}, \lambda) & b_2(\lambda) \end{bmatrix}, \tag{5.43}$$

$$b_1(\lambda) \;=\; -\frac{c_0(\lambda)}{s_0(\lambda)} - \frac{c_1(\lambda)}{s_1(\lambda)} - \frac{c_2(\lambda)}{s_2(\lambda)} - \alpha_1\,, \qquad b_2(\lambda) \;=\; -\frac{s_0'(\lambda)}{s_0(\lambda)} - \frac{s_1'(\lambda)}{s_1(\lambda)} - \frac{s_2'(\lambda)}{s_2(\lambda)} - \alpha_2\,, \tag{5.44}$$

$$w(z, \lambda) \;=\; \frac{1}{s_0(\lambda)} + \frac{z_1}{s_1(\lambda)} + \frac{z_2}{s_2(\lambda)}\,. \tag{5.45}$$

This is the function $w(z, \lambda)$ in (4.33). Notice that $w(z, \lambda)$ depends only on the potentials $q_i(x)$ through their Dirichlet spectrum since only the functions $s_i(\lambda)$ appear in the definition of $w(z, \lambda)$. The dispersion function for $(\mathring{\Gamma}, \mathring{A})$ is

$$D(z_1, z_2, \lambda) \;=\; \det \mathring{\hat{A}}(z_1, z_2, \lambda) \;=\; b_1(\lambda)b_2(\lambda) - \zeta(z, \lambda), \tag{5.46}$$

in which

$$\zeta(z, \lambda) \;=\; w(z, \lambda)w(z^{-1}, \lambda). \tag{5.47}$$

Observe that the dispersion functions of two different single-layer sheets of graphene have the same $\zeta(z,\lambda)$ exactly when corresponding edges are isospectral, because knowing the Dirichlet spectrum of a potential is equivalent to knowing its $s(\lambda)$ function [52, Ch. 2 Theorem 5].

All three edges in a period of a single layer are isospectral exactly when $s_0(\lambda) = s_1(\lambda) = s_2(\lambda)$, and in this case $\zeta(z,\lambda)$ separates as

$$\zeta(z,\lambda) \;=\; s_0(\lambda)^{-2} G(z_1,z_2), \tag{5.48}$$

in which

$$G(z_1,z_2) \;=\; (1+z_1+z_2)(1+z_1^{-1}+z_2^{-1}). \tag{5.49}$$

The Fermi surface of a single layer at energy λ is given by $D(z_1,z_2,\lambda)=0$, which reduces to

$$\Delta(\lambda) \;:=\; s_0(\lambda)^2\, b_1(\lambda) b_2(\lambda) \;=\; G(z_1,z_2). \tag{5.50}$$

We call $\Delta(\lambda)$ the "characteristic function" for this single-layer graphene model.

For $(z_1,z_2) = (e^{ik_1}, e^{ik_2})$ on the torus $\mathbb{T}^2$,

$$\begin{aligned} \tilde{G}(k_1,k_2) \;:=\; G(e^{ik_1},e^{ik_2}) \;&=\; \left|1+e^{ik_1}+e^{ik_2}\right|^2 \\ &=\; 1+8\cos\frac{k_2-k_1}{2}\cos\frac{k_1}{2}\cos\frac{k_2}{2}, \end{aligned} \tag{5.51}$$

and this has range $[0,9]$ as a function of real k_1 and k_2, with its minima occuring at $\pm(2\pi/3, -2\pi/3)$ [38, Lemma 3.3]. Thus the bands of this graphene model are the real λ-intervals over which $\Delta(\lambda)$ lies in $[0,9]$.

Single-layer quantum-graph graphene sheets and tubes, with a common symmetric potential $q_0(x)$ on all edges, are treated in detail in [38]. In this case, $b_1(\lambda) = b_2(\lambda)$ and the spectrum of the sheet is identical to that of the periodic Hill operator with potential $q_0(x)$ on a period. In contrast to the Hill operator, the dispersion relation exhibits conical singularities, one for each energy λ where $\Delta(\lambda)=0$. Fig. 6 shows a graph of $\Delta(\lambda)$. Conical singularities are discussed in section 5.7.

Notice that $\Delta(\lambda)$ is a non-negative function of real λ that has a minimum value of 0 (Fig. 6). The quadratic nature of the function at the minima is responsible for the Dirac cones, as explained in [38]. There is a close connection between the dispersion functions of discrete (tight-binding) models and quantum-graph models [38, Remark 3.2]. In the discrete graph model of single-layer graphene with a common interaction strength between atoms, the characteristic function reduces to $\Delta(\lambda) = 9\lambda^2$, and thus there is a Dirac cone at $\lambda = 0$. For multi-layer graphene in the discrete and quantum versions, $\Delta(\lambda)$ becomes a more complicated function of λ. Our analysis treats very general potentials on the three edges of a fundamental domain, and this leads to a more general dispersion function that is not separable into λ-dependent and z-dependent terms because the edges no longer in general possess a common $s(\lambda)$ function (see (5.46) and (5.48)).

5.2 Shifting and rotating

We adopt terminology on shifted layers of graphene that is used in the literature. The hexagonal graphene structure is invariant under translation by the sum $\xi_1+\xi_2$ of the two elementary shift vectors, as illustrated in Fig. 5. The shift by $(\xi_1+\xi_2)/3$ (dashed blue) places vertex v_2 onto vertex v_1 and places vertex v_1 onto the center of the hexagon; this will be called the B-shift. The shift by $2(\xi_1+\xi_2)/3$ (or $-(\xi_1+\xi_2)/3$, dotted orange) places v_1 onto v_2 and v_2 onto the center of the hexagon; this will be called the C-shift. The unshifted graph is called the A-shift.

By rotating the graphene structure by π about the center of an edge, the potentials reverse direction. This is illustrated on the right of Fig. 5, in which rotation is about the edge labeled 0. Each labeled oriented edge corresponds to a potential $q_i(x)$, with the parameter x increasing in the direction of the arrow. The labels 0, 1, 2 are preserved under rotation, but their orientations are reversed. Equivalently, rotation effects the change $q_i(x) \mapsto q_i(1-x)$ of the potentials. The rotation also switches the Robin conditions on the two vertices of a period.

Denote a single layer by $(\mathring{\Lambda}, \mathring{A})$ and its 180° rotation by $(\mathring{\Lambda}, \mathring{A}_\pi)$. The potentials $q_i(x)$ and $q_i(1-x)$ have the same Dirichlet spectrum, which coincides with the roots of the function $s_i(\lambda)$. Therefore the function $w(z,\lambda)$ in (5.45) is the same for both quantum graphs and their dispersion functions are polynomials in the same composite Floquet variable $\zeta(z,\lambda) = w(z,\lambda)w(z^{-1},\lambda)$.

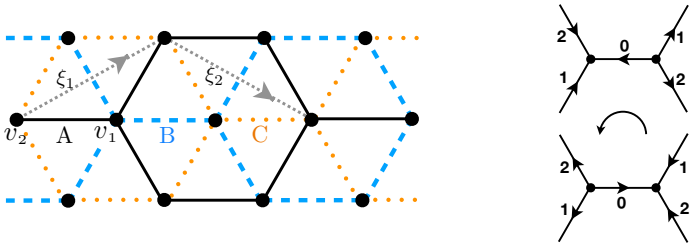

Figure 5: Left: A- B- and C-shifts of graphene are illustrated in solid black, dashed blue, and dotted orange, as described in the text. Right: Rotating graphene by 180° reverses the orientation of the potentials but preserves their Dirichlet spectra.

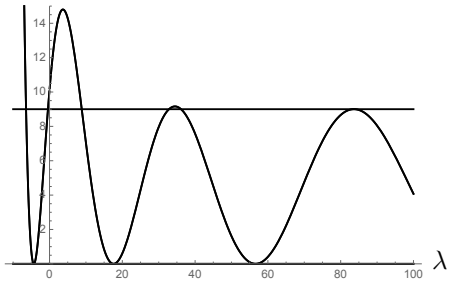

Figure 6: Graph of the characteristic function $\Delta(\lambda)$ of single-layer graphene, showing the first three spectral bands and the first three gaps. The bands are the λ-intervals for which $\Delta(\lambda) \in [0,9]$, which is the range of the function $\tilde{G}(k_1,k_2)$. The points where $\Delta(\lambda) = 0$ correspond to conical singularities of the dispersion relation $D(e^{ik_1}, e^{ik_2}, \lambda) = 0$, which occur inside the bands, as discussed in section 5.7 and [38]

5.3 AA-stacking and rotation

In AA-stacked graphene, each layer is stacked directly over the previous and each pair of vertically successive vertices is connected by an edge, as in Fig. 7. As a type-2 n-layer graph, the red vertices in a given period, together with the n–1 edges connecting them, form the connector graph (Σ_1, B_1), and the green vertices and the edges connecting them form (Σ_2, B_2). The hypotheses of Theorem 10 allow the potentials $q(x)$ on any pair of vertically aligned edges on two different layers to differ as long as the operators $-d^2/dx^2 + q_e(x)$ possess the same Dirichlet spectrum. The theorem then guarantees that the Fermi surface of the layered structure is reducible with n components.

A particular instance of AA-stacked graphene satisfying the hypotheses of the theorem is constructed from copies of a given single layer and its rotations about the center of an edge. Let a single layer (Λ, A_0) with arbitrary potentials on the three edges of a period and arbitrary Robin parameters on the two vertices be given. Rotation of this graph by 180° about the center of an edge, as described in the previous section and illustrated in Figs. 5,7 (right), results in a new layer of graphene (Λ, A_π) with the same underlying graph Λ but with the potentials oriented in the opposite direction and the Robin parameters at the two vertices switched.

Thus Theorem 10 applies to an n-layer stack, with each layer being either $(\mathring{\Lambda}, \mathring{A})$ or $(\mathring{\Lambda}, \mathring{A}_\pi)$, in any order, stacked in the AA sense. The Fermi surface of this n-layer graphene has n components. According to section 4.2, equation (4.40), the relation $D(z, \lambda) = 0$ reduces to n components

$$\mu_i(\lambda) \;=\; G(z_1, z_2) \qquad i = 1, \ldots, n, \tag{5.52}$$

in which μ_i are the eigenvalues of the "characteristic matrix"

$$\Delta(\lambda) \;=\; s_0(\lambda)^2\, \tilde{B}_1(\lambda)\tilde{B}_2(\lambda), \tag{5.53}$$

which generalizes the characteristic function (5.50) by the same name for the single layer.

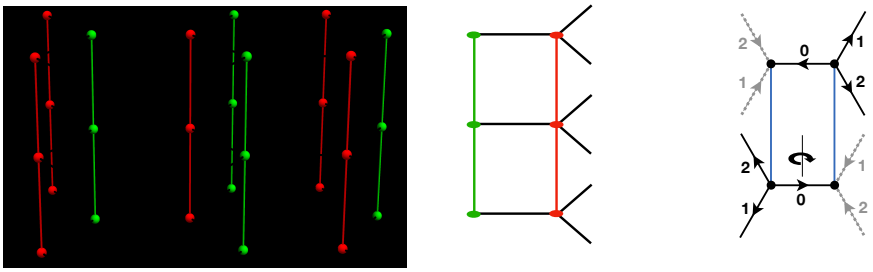

Figure 7: AA-stacked graphene in three layers and a fundamental domain thereof. If the potentials on corresponding edges on different layers have the same Dirichlet spectrum, then the Fermi surface for the multi-layer graph is reducible. This occurs, in particular, when a layer is rotated by π about the center of an edge.

Examples. (Fig. 8 and 9) Let the layers be identical with identical potential $q_0(x)$ on all three edges of a period. We take $q_0(x)$ to be symmetric about $x = 1/2$ so that the DtN map for the edge is independent of the direction. We choose

$$q_0(x) \;=\; -16\,\chi_{[1/3,2/3]}(x) \tag{5.54}$$

($\chi_Y(x)$ is the characteristic function of the set $Y \subset \mathbb{R}$) so that the DtN map is explicitly computable and so that the spectrum of the single layer does have gaps (because $q_0(x)$ is not constant; see [38]).

On all of the connector edges, which are all of length 1, we take the potential $q_c(x)$ to be either 0 or $q_0(x)$ or

$$q_c(x) \;=\; -10\,\chi_{[1/2,1]}(x), \tag{5.55}$$

which is not symmetric about the center. Fig. 8 and 9 show graphs of $\mu_i(\mu)$ for bi-layer and tri-layer graphene. Each eigenvalue contributes a sequence of bands and gaps to the spectrum of the multi-layer graph—the bands for the i^{th} sequence are the λ-intervals for which $\mu_i(\lambda) \in [0, 9]$. When the Dirichlet spectral function $s(\lambda)$ on the connecting edges is different from that of the layers, new thin bands are introduced. Conical singularities, or Dirac cones, are discussed below. These are

characteristic features of single-layer graphene, and in special cases of AA-stacking, they persist, according to Proposition 11. The recent article [21] also observes by computation that a finite number of AA-stacked graphene layers with the same symmetric potential on all edges within each layer and with symmetric connecting potentials, always exhibits Dirac cones. These Dirac cones can also be deduced from the full hexagonal symmetry group, as proved in [10].

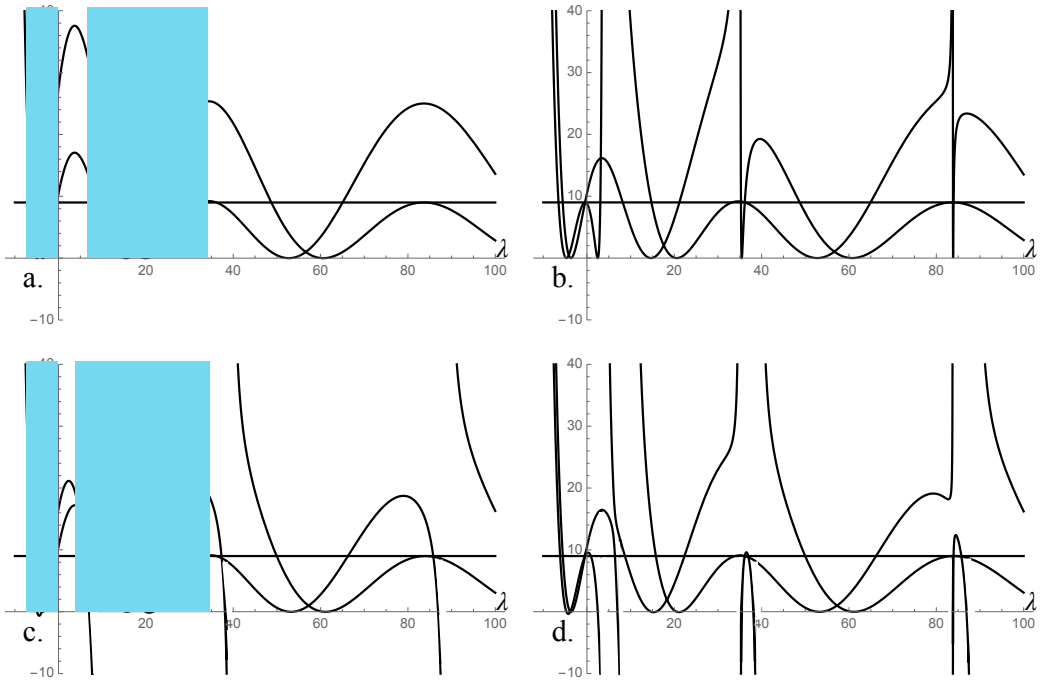

Figure 8: For double-layer AA-stacked graphene, the two eigenvalues $\mu_i(\lambda)$ $(i = 1, 2)$ of the characteristic matrix $\Delta(\lambda)$ give two sets of spectral bands and gaps. The bands are the λ-intervals for which $\mu_i(\lambda) \in [0, 9]$. The dispersion relation for the shaded λ-intervals are shown in Fig. 14. **a.** The connecting edges have the same potential as those of the layers (5.54). **b.** The potentials (5.55) of the two connecting edges are equal to each other but different from that of the layers (5.54). This creates additional thin bands (within each of the sets of spectral bands), which have conical singularities of their own. **c.** The potentials of the two connecting edges are different from each other ($q(x) = 0$ and 5.54). This destroys conical singularities and introduces additional thin gaps in their place. Additionally, new thin bands are introduced just below the vertical asymptotes. **d.** The potentials of the two connecting edges are different from each other ($q(x) = 0$ and 5.55).

5.4 AB-stacking

In AB-stacked graphene, also called Bernal stacking, the layers are in the A-shift or the B-shift and are coupled by a single edge per period. We allow any number of layers with the A- and B-shifts arranged in arbitrary order (such as ABABA, ABBA, *etc.*). Fig. 10 illustrates three layers with alternating shifts.

In each layer, we allow both $(\mathring{\Lambda}, \mathring{A})$ and $(\mathring{\Lambda}, \mathring{A}_\pi)$ or any potentials $q_i(x)$ $(i = 1, 2, 3)$ as long as, for each i, the Dirichlet spectra are invariant across layers. As noted above, this guarantees that the function $\zeta(z, \lambda)$ is independent of the layer since it depends only on the Dirichlet spectral functions $s_i(\lambda)$, which are equivalent to the Dirichlet spectra of the potentials $q_i(x)$. Note that isospectrality (which is explicitly required for type 2) arises for graphene in type-1 stacking. Thus the dispersion

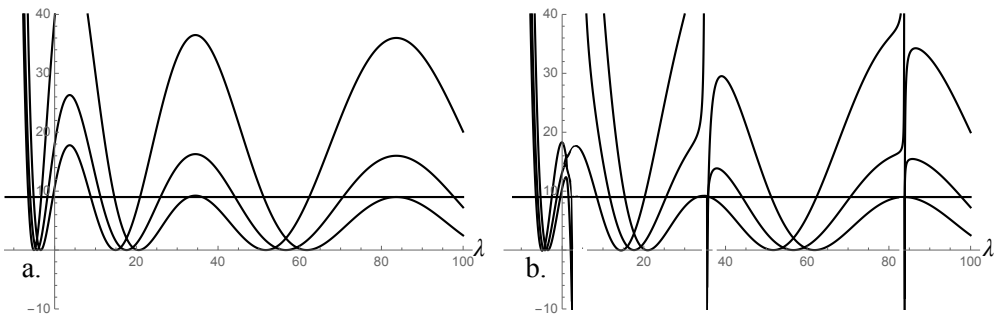

Figure 9: The three eigenvalues $\mu_i(\lambda)$ $(i = 1, 2, 3)$ of the characteristic matrix $\Delta(\lambda)$ for triple-layer AAA-stacked graphene, giving three sets of spectral bands and gaps. The bands are the λ-intervals for which $\mu_i(\lambda) \in [0, 9]$. **a.** The connecting edges have the same potential as those of the layers. **b.** The connecting edges have potential (5.54) at vertex v_1 and potential (5.55) at vertex v_2; this creates additional thin gaps and destroys Dirac cones (the minima are slightly below 0).

function of each layer is of the form (5.46) with different $b_i(\lambda)$ but the same $\zeta(z, \lambda)$. In any period of this layered structure, n vertices, one per layer, are aligned along a vertical line, and these are connected by edges. These vertices serve as vertices of separation of the individual layers. Thus Theorem 7 on type-1 multi-layer graphs applies.

Computations of AB-stacking in [20], with a common symmetric potential on all edges of each layer, show that three layers result in a Dirac cone (linear point), whereas two layers result in two bands touching quadratically (parabolic point). This raises the question as to whether the parity of the number of layers determines whether the touching point is linear or parabolic and whether symmetry arguments can be used to illuminate this question.

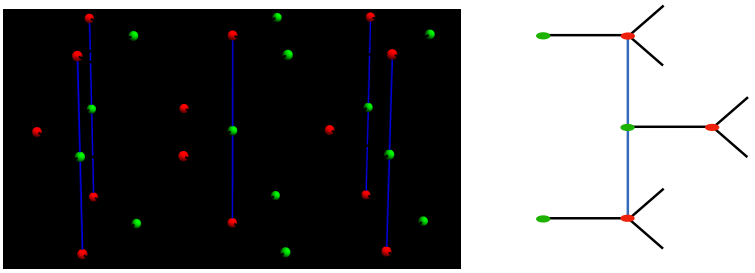

Figure 10: AB-stacked graphene in three layers (ABA) and a fundamental domain thereof.

Examples. (Fig. 11) As in the previous subsection, let the layers be identical with identical symmetric potential $q_0(x)$ on all edges. Fig. 11 shows the graphs of the roots $\mu_i(\lambda)$ of the polynomial $P(\zeta, \lambda)$—see Theorems 7 and 9. Conical singularities of the dispersion relation are discussed below in Section 5.7.

5.5 ABC-stacking

In ABC-stacked graphene, all three shifts are stacked, as illustrated in Fig. 12. The number of components of the Fermi surface of the ABC-stacked structure is equal to the number of layers. We leave the details of how to use Theorems 7 and 10 to prove this to the reader. The arguments are similar to those described for the more general mixed stacking below.

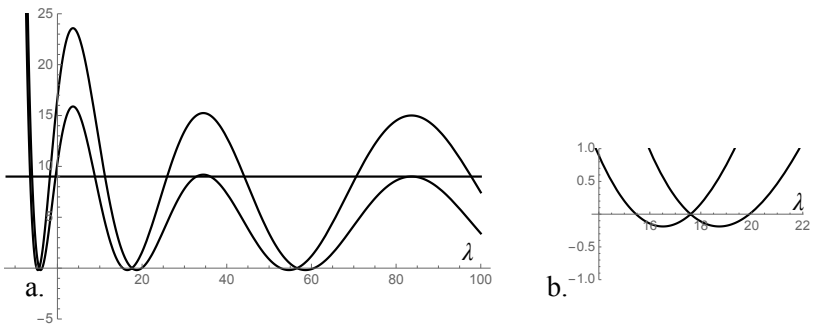

Figure 11: For double-layer AB-stacked graphene, these are graphs of $s(\lambda)^2\mu_i(\lambda)$ $(i = 1, 2)$, where $\mu_i(\lambda)$ are the two roots of $P(\zeta(z, \lambda), \lambda)$, as in Theorem 10. Each root gives a set of spectral bands and gaps. The bands are the λ-intervals for which $\mu_i(\lambda) \in [0, 9]$. **a.** The connecting edge has the same potential as those of the layers. **b.** A close view near $\lambda = 20$ shows that the graphs of $\mu_i(\lambda)$ cross the horizontal axis, and thus Dirac cones are not present.

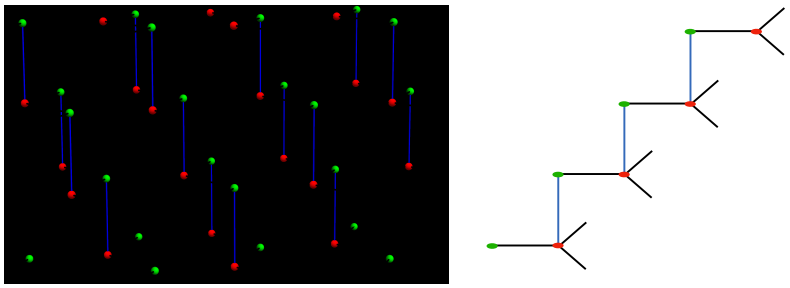

Figure 12: ABC-stacked graphene in four layers and a fundamental domain thereof.

5.6 Mixed stacking

Several graphene sheets can be stacked with arbitrary shifts (A,B,C) to obtain a mixed-stacking multi-layer sheet of graphene with reducible Fermi surface, as long as all the individual layers have dispersion function that is a polynomial in the same composite Floquet variable $\zeta(z, \lambda)$. As discussed above, this occurs when all vertically aligned edges are Dirichlet-isospectral. Fig. 13 depicts five layers stacked with mixed shifts. The dispersion function is a polynomial in $\zeta(z, \lambda)$ whose degree is the number of single sheets of graphene in the stack. The proof of this uses iterated application of the theorems on type-1 and type-2 multi-layer constructions and section 3.2, as described next.

Let Σ_1 and Σ_2 be n-layer and m-layer AA-stacked graphene quantum graphs (type 2). Let the individual layers of both have dispersion functions that are polynomials in a common $\zeta(z, \lambda)$. Let u_1 and u_n be corresponding (vertically aligned) vertices in the first and n-th layers of Σ_1, and let v_1 and v_m be corresponding vertices in the first and m-th layers of Σ_2.

Observe that $\Sigma_1^{u_n}$ has dispersion function that is also a function of the same $\zeta(z, \lambda)$. This is because a single graphene layer is separable at any vertex, and thus $\Sigma_1^{u_n}$ can be viewed as a type-2 $(n-1)$-layer graph with connectors that consist of the edges between the $n-1$ layers plus decorations. The same is true of $\Sigma_2^{v_0}$. Therefore Σ_1 and Σ_2 can be coupled by an edge between u_n and v_0 according to a two-layer type-1 construction, resulting in a quantum graph Γ with dispersion function that is a polynomial in $\zeta(z, \lambda)$.

This construction could just as well be carried out using $\Sigma_2^{v_m}$ in place of Σ_2, resulting in Γ^{v_m},

whose dispersion function is a polynomial in $\zeta(z,\lambda)$. Now yet another AA-stacked multi-layer graphene construction Σ_3 with the same $\zeta(z,\lambda)$ can be attached to Γ, and so on. These arguments need to modified somewhat if any of the AA-stacked sections Σ_i consists of only one layer, as in ABC-stacked graphene.

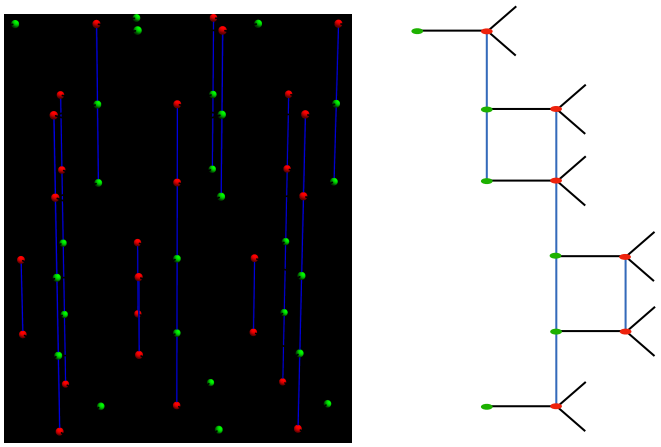

Figure 13: Five layers of graphene in mixed stacking, and a fundamental domain thereof.

5.7 Conical singularities

Single-layer graphene is famous for the "Dirac cone" feature of its dispersion relation $D(e^{ik_1}, e^{ik_2}, \lambda) = 0$. The Dirac cone is a conical singularity in (a branch of) the dispersion relation $D(\bar{k}, \lambda) = 0$ ($\bar{k} = (k_1, k_2)$), where it has the approximate form

$$(\lambda - \lambda_0)^2 \;\approx\; c\left|\bar{k} - \bar{k}_0\right|^2 \tag{5.56}$$

($c > 0$) to leading order for $(\bar{k}, \lambda)$ near $(\bar{k}_0, \lambda_0)$. There is a large amount of literature on this, for example [1, 16, 15, 47, 49, 51]. For Schrödinger operators in $\mathbb{R}^2$ with very general honeycomb-type potentials, the existence of circular Dirac cones and their stability is proved by perturbation methods in [30]. In [10], the authors provide a treatment for more general operators with hexagonal periodicity that is highlights the representations of various symmetry groups.

For single-layer graphene with equal and symmetric potentials on all edges, conical singularities occur at energies λ for which $\Delta(\lambda) = 0$ [38]. This is because the dispersion relation is $\Delta(\lambda) = \tilde{G}(k_1, k_2)$ and both $\Delta(\lambda)$ and $\tilde{G}(k_1, k_2)$ have 0 as nondegenerate minima (here, $\tilde{G}(k_1, k_2) := G(e^{ik_1}, e^{ik_2})$). The quasimomenta at these points are $\pm(2\pi/3, -2\pi/3)$.

When n layers are stacked in the AA sense, the n branches of the dispersion relation are $\mu_i(\lambda) = \tilde{G}(k_1, k_2)$ (5.52). When the connecting graph (sequence of connecting edges in this case) for the red vertices is the same as that for the green vertices, then $B_1(\lambda) = B_2(\lambda)$. The symmetry of the potentials about the centers of the edges implies $c(\lambda) = s'(\lambda)$; this, together with equal Robin parameters for each layer results in $\mathbf{b}_1(\lambda) = \mathbf{b}_2(\lambda)$. Thus $\tilde{B}_1(\lambda) = \tilde{B}_2(\lambda)$, and the $\mu_i(\lambda)$ are eigenvalues of the positive matrix $\Delta(\lambda)$ (5.53). Therefore, in each spectral band, $\mu_i(\lambda)$ reaches its minimal value of 0, and a conical singularity occurs (as long as the minima are nondegenerate), as shown in Fig. 8(a,b) and Fig. 9(a)—this is stated in the next proposition.

Proposition 11 (Condition for conical singularities)**.** *For an AA-stacked multi-layer graphene structure: if (1) the potentials on all the edges of all layers (black edges in Fig. 7) are identical and symmetric about the center of the edge; (2) in each layer, the two Robin parameters are equal; and (3) the potentials connecting the green vertices (green edges in Fig. 7) are the same as those connecting the red vertices (red edges in Fig. 7), then the dispersion relation has a conical singularity at each energy λ for which an eigenvalue $\mu(\lambda)$ of $\Delta(\lambda)$ is equal to zero and the second derivative of $\mu(\lambda)$ is nonzero.*

This proposition can also be obtained from [10, Theorem 2.4], as the conditions imply symmetry under rotation by $\pi/3$, inversion, and reflection, in the plane of the layers.

Incidentally, condition (1) in Proposition 11 apparently cannot be relaxed. The proof relies on two conditions on the potentials of the layers: They must all be isospectral and they must be symmetric. It is known (see [52]) that the Dirichlet spectrum completely determines the potential $q(x)$ within the class of symmetric potentials. Therefore all potentials on all the layers must be equal.

When the green and red vertices are connected differently, $\tilde{B}_1(\lambda)\tilde{B}_2(\lambda)$ is not necessarily a positive matrix, and indeed the $\mu_i(\lambda)$ cross 0 linearly, at which points there are nondegenerate band edges. This is illustrated in Fig. 8(c,d) and Fig. 9(b). Dispersion relations in (k_1, k_2, λ)-space are shown in Fig. 14.

For AB-stacked graphene, the numerical computation in Fig. 11(a,b) shows $\mu_i(\lambda)$ crossing 0 linearly at each point where it vanishes, and thus each of these points corresponds to a nondegenerate band edge (and not a conical singularity).

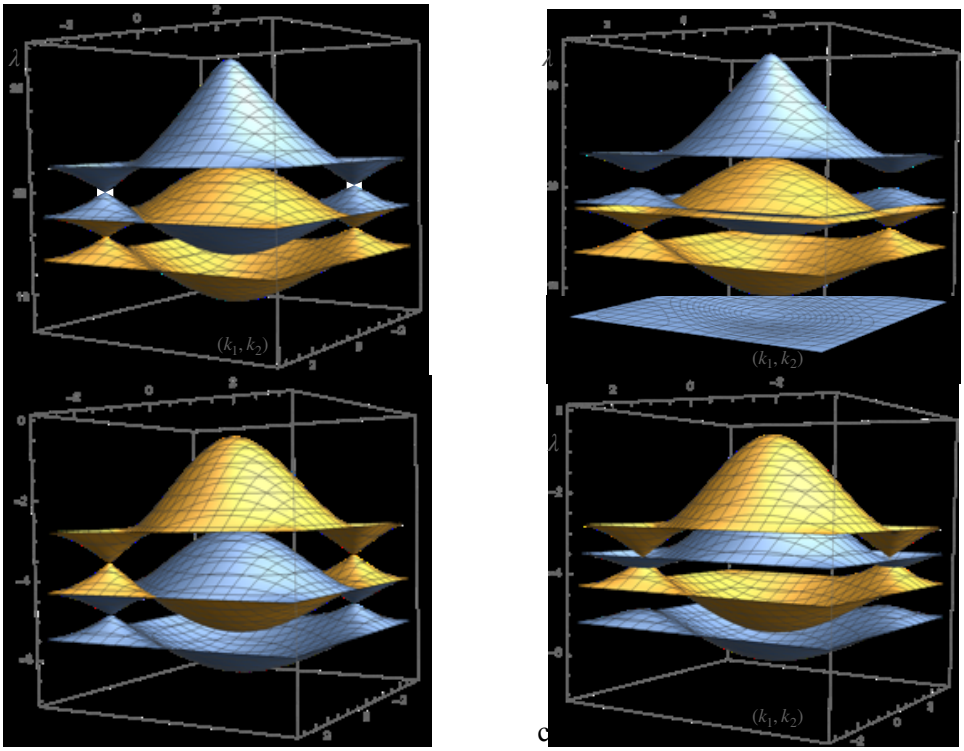

Figure 14: The dispersion relations for AA-stacked graphene from examples (a) and (c) in Fig. 8, shown for energies λ within the shaded intervals in Fig. 8(a,c). The two sets of bands coming from the eigenvalues $\mu_i(\lambda)$ $(i = 1, 2)$ are in blue and yellow. **a.** The two connecting edges have the same potential. Each of the energies λ where the $\mu_i(\lambda)$ hit zero in Fig. 8(a) exhibits a conical singularity at two different quasimomenta (k_1, k_2). **c.** The two connecting edges have different potentials. All of the conical points open into gaps. In the upper interval, an additional thin band appears.

6 Some irreducible Fermi surfaces

We give two examples of multi-layer quantum graphs that are not of type 1 or type 2 and whose Fermi surface is not reducible for some open set of energies.

The first example is a bi-layer graph with identical tripartite layers; the single layer is shown in Fig. 15. Each edge of the single layer has the same symmetric potential. Two copies of this layer are connected by two edges per period, one edge between green vertices and one between red, and these two edges have potentials from different asymmetry classes as defined in [60] (otherwise the Fermi surface would be reducible by [60, Theorem 4]). With the vertices ordered green-red-blue,

the spectral matrix for this graph is

$$\hat{A}(z,\lambda) = \frac{1}{s(\lambda)} \begin{bmatrix} -3c(\lambda) & 0 & 1+z_2 & 0 & 1 & 0 \\ 0 & -3c(\lambda) & 0 & 1+z_2 & 0 & 1 \\ 1+z_2^{-1} & 0 & -2c(\lambda)-2s'(\lambda) & 0 & 1+z_1 & 0 \\ 0 & 1+z_2^{-1} & 0 & -2c(\lambda)-2s'(\lambda) & 0 & 1+z_1 \\ 1 & 0 & 1+z_1^{-1} & 0 & -3s'(\lambda) & 0 \\ 0 & 1 & 0 & 1+z_1^{-1} & 0 & -3s'(\lambda) \end{bmatrix} \tag{6.57}$$

$$+ \begin{bmatrix} -c_1(\lambda)s_1(\lambda)^{-1} & s_1(\lambda)^{-1} & 0 & 0 & 0 & 0 \\ s_1(\lambda)^{-1} & -s_1'(\lambda)s_1(\lambda)^{-1} & 0 & 0 & 0 & 0 \\ 0 & 0 & -c_2(\lambda)s_2(\lambda)^{-1} & s_2(\lambda)^{-1} & 0 & 0 \\ 0 & 0 & s_2(\lambda)^{-1} & -s_2'(\lambda)s_2(\lambda)^{-1} & 0 & 0 \\ 0 & 0 & 0 & 0 & 0 & 0 \\ 0 & 0 & 0 & 0 & 0 & 0 \end{bmatrix}. \tag{6.58}$$

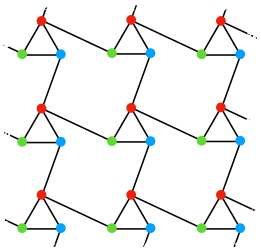

Figure 15: A tripartite periodic graph. Two layers of this graph coupled at the green and red vertices with appropriate potentials yields an irreducible Fermi surface for some energies.

We prove, with the help of a computer, that the determinant of this matrix is not factorable as a product of non-monomial Laurent polynomials in z_1 and z_2. Lemma 12 below guarantees that, given $\lambda \in \mathbb{R}$ and three real numbers α, β and γ, with $\alpha\beta \neq 0$, there exists a continuous real potential $q(x)$ whose spectral functions satisfy $c(\lambda) = \alpha$, $s(\lambda) = \beta$, and $s'(\lambda) = \gamma$. Thus, we can choose the values of $c(\lambda)$, $s(\lambda)$, $s'(\lambda)$, $c_1(\lambda)$, $s_1(\lambda)$, $s_1'(\lambda)$, $c_2(\lambda)$, $s_2(\lambda)$ and $s_2'(\lambda)$ independently, and the determinant becomes a Laurent polynomial in z_1 and z_2 with real coefficients. Nonfactorability occurs, for example, for $c = s = s' = s_1 = s_1' = c_1 = s_2 = s_2' = 1$ and $c_2 = 2$, and therefore also for an open set of energies around λ for the same potentials.

The second example is crossed bi-layer graphene. The layers are identical, and, within one period, the red vertex of each layer is connected to the green vertex of the other layer. With

$w = 1 + z_1^{-1} + z_2^{-1}$ and $w' = 1 + z_1 + z_2$ the spectral matrix for this graph is

$$\hat{A}(z,\lambda) \;=\; \frac{1}{s(\lambda)} \begin{bmatrix} -3c(\lambda) & 0 & w & 0 \\ 0 & -3c(\lambda) & 0 & w \\ w' & 0 & -3s'(\lambda) & 0 \\ 0 & w' & 0 & -3s'(\lambda) \end{bmatrix} \tag{6.59}$$

$$+ \begin{bmatrix} -c_1(\lambda)s_1(\lambda)^{-1} & 0 & 0 & s_1(\lambda)^{-1} \\ 0 & -c_2(\lambda)s_2(\lambda)^{-1} & s_2(\lambda)^{-1} & 0 \\ 0 & s_2(\lambda)^{-1} & -s_2'(\lambda)s_2(\lambda)^{-1} & 0 \\ s_1(\lambda)^{-1} & 0 & 0 & -s_1'(\lambda)s_1(\lambda)^{-1} \end{bmatrix}. \tag{6.60}$$

The choice $c = s = s' = s_1 = s_1' = c_1 = s_2 = s_2' = 1$ and $c_2 = 2$ renders the determinant not factorable. Incidentally, when the connecting edges have the same potential, the determinant factors, but the factors are not functions of ww' or any other function of z_1 and z_2.

7 Embedded eigenvalues

In this section, we show how the reducibility of the Fermi surface can be exploited to create a local defect of a periodic quantum graph operator that engenders a bound (L^2) state at an energy within the continuous spectrum, and such that this state has unbounded support. Such an energy is an embedded eigenvalue of the operator. The condition of unbounded support distinguishes these eigenvalues from the energies of the flat bands, discussed in Section 2.6, which are peculiar to graph operators, both discrete and quantum. See more discussion of this interesting issue in [40].

We discussed in the Introduction that irreducibility of the Fermi surface is an obstruction to the existence of embedded eigenvalues with unbounded support. The proof of this in [40] gives guidance on how to construct embedded eigenvalues when one does have reducibility. The key is in the Floquet transform, where the dispersion function $D(z,\lambda) = D_1(z,\lambda)D_2(z,\lambda)$ appears in the denominator. The strategy is to choose an energy λ such that exactly one of the factors, say $D_1(z,\lambda)$ but not $D_2(z,\lambda)$, vanishes at some z values on the torus $\mathbb{T}^2 \subset \mathbb{C}^2$. This means that λ lies in the set of spectral bands contributed by $D_1(z,\lambda)$ but outside the bands contributed by $D_2(z,\lambda)$. Then one arranges a defect so that only the factor $D_1(z,\lambda)$ is cancelled in the solution. We carry this out here for bilayer graphene in AA- and AB- stacking.

Let the potentials on all of the edges be $q_e(x) = 0$. The spectral matrix for the single layer is

$$\hat{\mathring{A}}(z,\lambda) \;=\; \frac{1}{s(\lambda)} \begin{bmatrix} -3c(\lambda) & w(z) \\ w(z^{-1}) & -3c(\lambda) \end{bmatrix}, \tag{7.61}$$

in which $s(\lambda) = \sin\sqrt{\lambda}$ and $c(\lambda) = \cos\sqrt{\lambda}$ and $w(z) = 1 + z_1 + z_2$. The spectral matrix (4.34) for AA-stacked graphene Γ_{AA} becomes

$$\hat{A}(z,\lambda) \;=\; \frac{1}{s(\lambda)} \begin{bmatrix} s(\lambda)\hat{\mathring{A}}(z,\lambda) - c(\lambda)I_2 & I_2 \\ I_2 & s(\lambda)\hat{\mathring{A}}(z,\lambda) - c(\lambda)I_2 \end{bmatrix}, \tag{7.62}$$

in which I_2 is the 2×2 identity matrix. The dispersion function $D(z,\lambda)$ is the determinant of this matrix, and since we will consider λ that is not a root of $s(\lambda)$, we may work with

$$\tilde{D}(z,\lambda) = \det\big(s(\lambda)\hat{A}(z,\lambda)\big) = \tilde{D}_1(z,\lambda)\tilde{D}_2(z,\lambda) \tag{7.63}$$

$$= \big(16c(\lambda)^2 - 8c(\lambda) + 1 - \zeta(z)\big)\big(16c(\lambda)^2 + 8c(\lambda) + 1 - \zeta(z)\big), \tag{7.64}$$

in which $\zeta(z) = w(z)w(z^{-1})$. The dispersion relations for the two components of the Fermi surface, as displayed in (5.52), therefore turn out to be

$$\zeta(z_1,z_2) \;=\; \mu_\pm(\lambda) \;:=\; 16c(\lambda)^2 \pm 8c(\lambda) + 1. \tag{7.65}$$

These two components contribute different sets of bands, say $\sigma_\pm(A)$, to the spectrum of the AA-stacked graphene model (σ_- corresponds to the factor $\tilde{D}_1(z,\lambda)$, and σ_+ to the factor $\tilde{D}_2(z,\lambda)$.). As described in Section 5.3, since the range of $\zeta(e^{ik_1},e^{ik_2})$ is the interval $[0,9]$, the bands are the inverse images of this interval by the functions $\mu_\pm(\lambda)$, whose graphs are shown in Fig. 16(left). Precisely, $\sigma_\pm(A) = \{\lambda : 16c(\lambda)^2 \pm 8c(\lambda) + 1 \in [0,9]\}$.

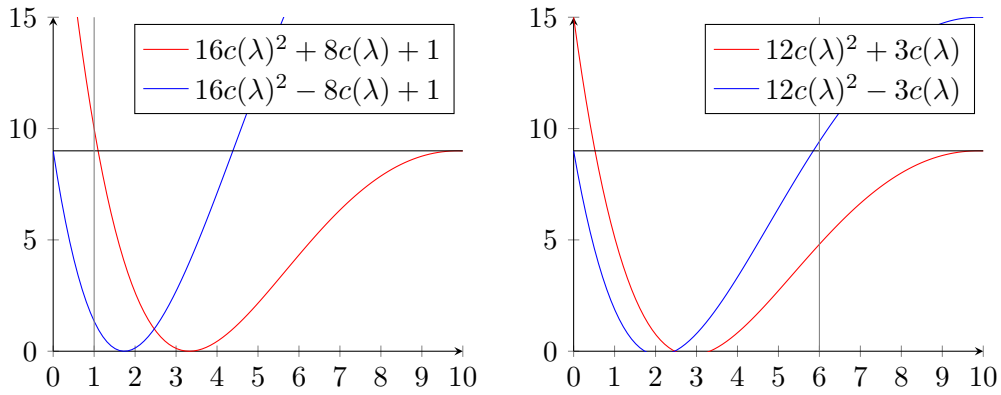

Figure 16: Two sets of spectral bands for bi-layer graphene (AA left; AB right), coming from the two components of the Fermi surface, are the inverse images of the interval $[0,9]$ under the two graphed dispersion functions. On the left, the vertical line shows that, for AA-stacking, the energy $\lambda=1$ lies within a band of the relation $G(k_1,k_2) = \mu_-(\lambda)$ but in a gap of the relation $G(k_1,k_2) = \mu_+(\lambda)$. Similarly, on the right, the energy $\lambda=6$ lies in exactly one of the sets of bands for AB-stacking.

Notice that $\lambda=1$, for example, lies in $\sigma_-(A)\setminus\sigma_+(A)$. We will show how to construct a local defect in Γ_{AA} and an embedded eigenvalue for the defective graph at any $\lambda \in \sigma_-(A)\setminus\sigma_+(A)$. At such a value of λ, we will first consider the following auxiliary problem for the discrete-graph reduction (sec. 2.2, p. 7) of the full quantum-graph operator on Γ_{AA},

$$\mathfrak{A}(\lambda)u \;=\; \phi, \tag{7.66}$$

where ϕ is a forcing function defined on the vertices of Γ_{AA} that is nonzero at only finitely many vertices. Its Floquet transform $\hat{\phi}(z)$ is therefore a Laurent polynomial in $z=(z_1,z_2)$, and its coefficients can be considered to be vectors in $\mathbb{C}^4$ since a fundamental domain W of Γ_{AA} contains four vertices. The solution u is the response (also defined on the vertices of Γ_{AA}) to the forcing function ϕ at energy λ. Its Floquet transform $\hat{u}(z)$ is obtained algebraically by

$$\hat{u}(z) \;=\; \hat{A}(z,\lambda)^{-1}\hat{\phi}(z) \;=\; \frac{\mathrm{Adj}(\hat{A}(z,\lambda))\hat{\phi}(z)}{D(z,\lambda)}, \tag{7.67}$$

in which $\mathrm{Adj}(\hat{A}(z,\lambda))$ is the adjunct of $\hat{A}(z,\lambda)$.

Let us now fix λ such that $s(\lambda) \neq 0$, say $\lambda = 1$ to be concrete, and choose the forcing function in the Fourier domain to be

$$\hat{\phi}(z) \;=\; \tilde{D}_1(z,1)\vec{c} \;=\; \big(16c(1)^2 - 8c(1) + 1 - \zeta(z_1,z_2)\big)\vec{c}. \tag{7.68}$$

Since $\hat{\phi}(z)$ is a Laurent polynomial in $z = (z_1, z_2)$, the forcing function ϕ on Γ_{AA} has compact support. Then we obtain

$$\hat{u}(z) \;=\; \frac{\mathrm{Adj}(\hat{A}(z,1))\,\vec{c}}{16c(1)^2 + 8c(1) + 1 - \zeta(z)}. \tag{7.69}$$

The response u has a value at each of the four vertices in each shift of W by any element of $g \in \mathbb{Z}^d$, and so u can be considered to be a function of $g \in \mathbb{Z}^d$ with values in $\mathbb{C}^4$. It is obtained by Fourier inversion,

$$u(g) \;=\; \frac{1}{(2\pi)^2} \int_{\mathbb{T}^2} z^g\, \hat{u}(z)\, dz, \tag{7.70}$$

in which $\mathbb{T}^2 = \{z \in \mathbb{C}^2 : |z_1| = |z_2| = 1\}$ is the two-dimensional torus in $\mathbb{C}^2$.

Since $\lambda = 1$ is not in $\sigma_2(A)$, the denominator does not vanish on the two-dimensional torus $\mathbb{T}^2 = \{z \in \mathbb{C}^2 : |z_1| = |z_2| = 1\}$ in $\mathbb{C}^2$. Therefore $\hat{u}(z)$ is analytic on $\mathbb{T}^2$, and it follows that $u \in L^2(\mathcal{V}(\Gamma_{AA}))$ (u is in fact exponentially decaying). As long as the denominator $\tilde{D}_2(z,1)$ is not cancelled identically by any of the four components of the vector in the numerator, $\hat{u}(z)$ will not be a Laurent polynomial in z. This means that u has unbounded support, that is, it is nonzero on infinitely many vertices. One can compute the values at the four vertices of each shift of W explicitly; for example, when $\vec{c} = [1,0,0,0]^t$,

$$\begin{aligned}
u_1(g) &= \frac{s(1)}{(2\pi)^2} \int_{\mathbb{T}^2} z^g \frac{-64c(1)^3 + 4c(1)\zeta(z)}{16c(1)^2 + 8c(1) + 1 - \zeta(z)} dz \\
u_2(g) &= \frac{s(1)}{(2\pi)^2} \int_{\mathbb{T}^2} z^g \frac{(1 + z_1 + z_2)(16c(1)^2 - 1 - \zeta(z))}{16c(1)^2 + 8c(1) + 1 - \zeta(z)} dz \\
u_3(g) &= \frac{s(1)}{(2\pi)^2} \int_{\mathbb{T}^2} z^g \frac{1 - \zeta(z) - 16c(1)^2}{16c(1)^2 + 8c(1) + 1 - \zeta(z)} dz \\
u_4(g) &= \frac{s(1)}{(2\pi)^2} \int_{\mathbb{T}^2} z^g \frac{8c(1)(1 + z_1 + z_2)}{16c(1)^2 + 8c(1) + 1 - \zeta(z)} dz,
\end{aligned}$$

and confirm that the denominator is not simultaneously a factor of all four of the numerators.

We now show how the solution u to $\mathfrak{A}(\lambda)u = \phi$ can be extended to an L^2 eigenstate of a local perturbation of the quantum graph A. For simplicity, let ϕ within a fundamental domain of Γ_{AA} be possibly nonzero only on the two vertices of a single edge $e\{v,w\}$. We will construct a perturbation of A obtained by replacing the potential $q_e(x)$ on the edge e by a different potential $V(x)$. This yields a perturbation (Γ_{AA}, A_V) of the periodic quantum graph (Γ_{AA}, A). Our task is to determine $V(x)$ so that the equation $A_V u = \lambda u$ for some extension of u to the edges of Γ_{AA} is equivalent to $\mathfrak{A}(\lambda)u = \phi$. The procedure that follows can be repeated to account for forcing on multiple edges.

Let $\mathfrak{A}_V(\lambda)u = 0$ be the discrete reduction of the eigenvalue problem $A_V u = \lambda u$ (sec. 2.2, p. 7). Then our task is reduced to finding $V(x)$ so that

$$\mathfrak{A}(\lambda)u = \phi \quad\Longleftrightarrow\quad \mathfrak{A}_V(\lambda)u = 0. \tag{7.71}$$

To do this, we must look at how the matrices $\mathfrak{A}(\lambda)$ and $\mathfrak{A}_V(\lambda)$ are constructed. They are indexed by $\mathcal{V}(\Gamma_{AA})$. The 2×2 submatrix of $\mathfrak{A}(\lambda)$ corresponding to the vertices $\{v,w\}$ of e has a contribution from the DtN map (2.8) with $g=0$ and $s_e(\lambda)=s(\lambda)$ (similarly for c and s'); and the corresponding 2×2 submatrix of $\mathfrak{A}_V(\lambda)$ has a similar contribution, but with $s_e(\lambda)=s_V(\lambda)$ (similarly for c and s') coming from the spectral functions for the operator $-d^2/dx^2+V(x)$. Otherwise, $\mathfrak{A}(\lambda)$ and $\mathfrak{A}_V(\lambda)$ are identical.

Given that $\mathfrak{A}(\lambda)u=\phi$, the task is to find $V(x)$ such that $\mathfrak{A}_V(\lambda)u=\mathfrak{A}(\lambda)u-\phi$. By the foregoing discussion and the fact that ϕ vanishes except at the vertices v and w, this equation holds automatically at all other vertices. Thus this equation reduces to

$$\frac{1}{s_V(\lambda)}\begin{bmatrix}-c_V(\lambda) & 1\\ 1 & -s_V'(\lambda)\end{bmatrix}\begin{bmatrix}u(v)\\ u(w)\end{bmatrix}=\begin{bmatrix}u'(v)-\phi(v)\\ u'(w)-\phi(w)\end{bmatrix}. \tag{7.72}$$

That there is a potential $V(x)$ that satisfies these equations for, say, $\lambda=1$, is settled by the lemma below.

In the case of AB-stacked graphene,

$$\hat{A}(z,\lambda) \;=\; \frac{1}{s(\lambda)}\begin{bmatrix}s(\lambda)A(z,\lambda)-c(\lambda)E_{22} & E_{22}\\ E_{22} & s(\lambda)A(z,\lambda)^T-c(\lambda)E_{22}\end{bmatrix}, \tag{7.73}$$

in which E_{22} is the 2×2 matrix with 1 in the $(2,2)$-entry and zero everywhere else. The dispersion relations for the two components of the Fermi surface turn out to be

$$\zeta(z_1,z_2) \;=\; \mu_\pm(\lambda) \;:=\; 12c(\lambda)^2\pm3c(\lambda). \tag{7.74}$$

The graphs of the functions $\mu_\pm(\lambda)$ are shown in Fig. 16(right), and $\lambda=6$ is seen to lie in the spectrum coming from $\mu_+(\lambda)$ and not in the spectrum coming from $\mu_-(\lambda)$. Again for $\vec{c}=[1,0,0,0]^t$, one computes the values of u at the vertices,

$$\begin{aligned}
u_1(g)&=\frac{s(6)}{(2\pi)^2}\int_{\mathbb{T}^2}z^g\frac{3c(6)-48c(6)^3-4c(6)\zeta(z)}{12c(6)^2-3c(6)+\zeta(z)}dz\\
u_2(g)&=\frac{s(6)}{(2\pi)^2}\int_{\mathbb{T}^2}z^g\frac{(1+z_1+z_2)(12c(6)^2-\zeta(z))}{12c(6)^2-3c(6)-\zeta(z)}dz\\
u_3(g)&=\frac{s(6)}{(2\pi)^2}\int_{\mathbb{T}^2}z^g\frac{-(1+z_1+z_2)^2}{12c(6)^2-3c(6)-\zeta(z)}dz\\
u_4(g)&=\frac{s(6)}{(2\pi)^2}\int_{\mathbb{T}^2}z^g\frac{3c(6)(1+z_1+z_2)}{12c(6)^2-3c(6)-\zeta(z)}dz
\end{aligned}$$

and confirms that the denominator is not canceled in all four expressions simultaneously. The rest of the construction of an embedded eigenvalue is essentially identical to the case of AA-stacking.

Lemma 12. *Given real numbers α, β, γ, and λ with $\alpha\beta\neq0$, there exists a real-valued potential $q(x)$ on $[0,1]$ for which $c(\lambda)=\alpha$, $s(\lambda)=\beta$, and $s'(\lambda)=\gamma$.*

Proof. Let $c(x;\lambda)$ be the solution to $-u''+q(x)u=\lambda u$ such that $c(0;\lambda)=1$ and $c'(0;\lambda)=0$; and let $s(x;\lambda)$ be the solution such that $s(0;\lambda)=0$ and $s'(0;\lambda)=1$. Then, by definition, $c(\lambda)=c(1;\lambda)$, $s(\lambda)=s(1;\lambda)$, and $s'(\lambda)=s'(1;\lambda)$, with the prime referring to d/dx. The ODE implies

$$q(x)-\lambda=\frac{c''(x;\lambda)}{c(x;\lambda)}. \tag{7.75}$$

We prescribe additionally that $c(x;\lambda)$ is an analytic function of x such that

1. $c(1;\lambda) = \alpha$ and $c'(1;\lambda) = \frac{\alpha\gamma - 1}{\beta}$,
2. $c(x;\lambda)$ has finitely many roots in $(0,1)$, and at each root the first derivative is nonzero and the second derivative is zero,
3. $\int_0^1 c(x;\lambda)^{-2} dx = \frac{\beta}{\alpha}$.

Let us show that the potential $q(x)$ obtained from this function $c(x;\lambda)$ is well defined and has the three desired properties.

Because of the second property, $c''(x;\lambda)/c(x;\lambda)$ is analytic at each zero of $c(x;\lambda)$. By construction $c(1;\lambda) = \alpha$. From the Wronskian identity $c(x;\lambda)s'(x;\lambda) - s(x;\lambda)c'(x;\lambda) = 1$, one obtains

$$s(x;\lambda) = c(x;\lambda) \int_0^x \frac{1}{c(x;\lambda)^2} dx, \tag{7.76}$$

which, together with properties (1) and (3), yields $s(1;\lambda) = \beta$. The Wronskian identity also gives

$$\alpha s' - \left(\frac{\alpha\gamma - 1}{\beta}\right)\beta = 1, \tag{7.77}$$

from which we obtain $s'(1;\lambda) = \gamma$. □

8 Appendix: Moving the poles of the dispersion function

This appendix proves Proposition 1 in section 2.1. The proof is based on the dotted-graph technique [41]. First consider the simple case of a quantum graph where the underlying graph E consists of two vertices and the edge $e\{v_1, v_2\}$ between them, identified with the x-interval $[0, L]$. With the operator $-d^2/dx^2 - q(x)$ and Robin parameters α_1 at $v_1(x = 0)$ and α_2 at $v_2(x = L)$, we obtain a quantum graph (E, Q). Let $\dot{E}$ be the graph obtained by placing an additional vertex v at the point of e corresponding to $x = \ell \in]0, L[$; thus $\dot{E}$ consists of three vertices and two edges $e_1\{v_1, v\}$ and $e_2\{v, v_2\}$, with e_1 identified with $[0, \ell]$ and e_2 identified with $[\ell, L]$.

Restricting the potential q to e_1 and e_2 and imposing the Neumann condition at v yields a quantum graph $(\dot{E}, \dot{Q})$. The Neumann condition guarantees continuity of value and derivative across v, and therefore (E, Q) and $(\dot{E}, \dot{Q})$ are essentially identical quantum graphs.

Denote the transfer matrices for $-d^2/dx^2 + q(x)$ on $[0, L]$, on $[0, \ell]$, and on $[\ell, L]$ by

$$T(\lambda) = \begin{bmatrix} c(\lambda) & s(\lambda) \\ c'(\lambda) & s'(\lambda) \end{bmatrix}, \quad T_1(\lambda) = \begin{bmatrix} c_1(\lambda) & s_1(\lambda) \\ c_1'(\lambda) & s_1'(\lambda) \end{bmatrix}, \quad T_2(\lambda) = \begin{bmatrix} c_2(\lambda) & s_2(\lambda) \\ c_2'(\lambda) & s_2'(\lambda) \end{bmatrix}. \tag{8.78}$$

Considering $(\dot{E}, \dot{Q})$ as one period of a d-periodic disconnected graph, its dispersion function is a meromorphic function of λ alone, as its discrete reduction $\hat{\dot{Q}}(z, \lambda)$ is independent of z. When Robin conditions are imposed at both endpoints, denote this function by $\dot{h}^{\mathrm{RR}}(\lambda) = \det \hat{\dot{Q}}(z, \lambda)$,

$$\dot{h}^{\mathrm{RR}}(\lambda) \;=\; \det \begin{bmatrix} -\frac{c_1(\lambda)}{s_1(\lambda)} - \alpha_1 & \frac{1}{s_1(\lambda)} & 0 \\ \frac{1}{s_1(\lambda)} & -\frac{s_1'(\lambda)}{s_1(\lambda)} - \frac{c_2(\lambda)}{s_2(\lambda)} & \frac{1}{s_2(\lambda)} \\ 0 & \frac{1}{s_2(\lambda)} & -\frac{s_2'(\lambda)}{s_2(\lambda)} - \alpha_2 \end{bmatrix}. \tag{8.79}$$

When the homogeneous Dirichlet condition is imposed at either end (not both ends) of $[0, L]$, with a Robin condition at the other end, one obtains

$$\dot{h}^{\mathrm{DR}}(\lambda) = \det \begin{bmatrix} -\frac{s_1'(\lambda)}{s_1(\lambda)} - \frac{c_2(\lambda)}{s_2(\lambda)} & \frac{1}{s_2(\lambda)} \\ \frac{1}{s_2(\lambda)} & -\frac{s_2'(\lambda)}{s_2(\lambda)} - \alpha_2 \end{bmatrix}, \quad \dot{h}^{\mathrm{RD}}(\lambda) = \det \begin{bmatrix} -\frac{c_1(\lambda)}{s_1(\lambda)} - \alpha_1 & \frac{1}{s_1(\lambda)} \\ \frac{1}{s_1(\lambda)} & -\frac{s_1'(\lambda)}{s_1(\lambda)} - \frac{c_2(\lambda)}{s_2(\lambda)} \end{bmatrix}, \tag{8.80}$$

and $\dot{h}^{\mathrm{DD}}(\lambda) = -\frac{s_1'(\lambda)}{s_1(\lambda)} - \frac{c_2(\lambda)}{s_2(\lambda)}$ when the Dirichlet condition is imposed at both ends. Using the relation $T = T_2 T_1$, one computes that

$$\dot{h}^{\mathrm{RR}} = -\frac{c' + \alpha_1 s' + \alpha_2 c + \alpha_1 \alpha_2 s}{s_1 s_2}, \quad \dot{h}^{\mathrm{DR}} = \frac{s' + \alpha_2 s}{s_1 s_2}, \quad \dot{h}^{\mathrm{RD}} = \frac{c + \alpha_1 s}{s_1 s_2}, \quad \dot{h}^{\mathrm{DD}} = -\frac{s}{s_1 s_2}. \tag{8.81}$$

For the un-dotted quantum graph (E, Q), one obtains these same expressions except with the denominator $s_1(\lambda)s_2(\lambda)$ replaced by $s(\lambda)$,

$$h^{\mathrm{RR}} = -\frac{c' + \alpha_1 s' + \alpha_2 c + \alpha_1 \alpha_2 s}{s}, \quad h^{\mathrm{DR}} = \frac{s' + \alpha_2 s}{s}, \quad h^{\mathrm{RD}} = \frac{c + \alpha_1 s}{s}, \quad h^{\mathrm{DD}} = -\frac{s}{s}. \tag{8.82}$$

Observe that, given λ_0, one can guarantee that $s_1(\lambda_0)s_2(\lambda_0) \neq 0$ by choosing the point ℓ not to be a root of any Dirichlet eigenfunction of $-d^2/dx^2 + q(x)$ for λ_0 on $[0, L]$.

These calculations show that the numerators in the expressions above contain the essential spectral information. In fact this is true of periodic quantum graphs in general. To go from the dispersion function for a quantum graph (Γ, A) to the dispersion function for a dotted version $(\dot{\Gamma}, \dot{A})$, one simply multiplies by a factor of the form $s(\lambda)/(s_1(\lambda)s_2(\lambda))$ for each dotted edge.

Proof of Proposition 1. If v_1 and v_2 are not in the same $\mathbb{Z}^d$ orbit, we can assume that they both are in the vertex set $\mathcal{V}_0$ of the fundamental domain chosen for constructing $\hat{A}(z, \lambda)$, since $D(z, \lambda)$ is independent of that choice. Denote by $\hat{A}(z, \lambda)$ and $\dot{\hat{A}}(z, \lambda)$ the discrete reductions at energy λ of the quantum graphs (Γ, A) and $(\dot{\Gamma}, \dot{A})$. Index the rows and columns of $\hat{A}(z, \lambda)$ so that the first two correspond to v_1 and v_2; then augment it with a 0^{th} column and a 0^{th} row consisting of a 1 in the leading entry and zeroes elsewhere. Call this matrix $\hat{\hat{A}}(z, \lambda)$.

The matrix $\hat{\hat{A}}(z, \lambda)$ has the block form

$$\left[\begin{array}{c|c} \Sigma + A & B \\ \hline C & D \end{array}\right], \tag{8.83}$$

in which

$$\Sigma = \begin{bmatrix} 1 & 0 & 0 \\ 0 & -cs^{-1} & s^{-1} \\ 0 & s^{-1} & -s's^{-1} \end{bmatrix}, \tag{8.84}$$

A and B have all zeroes in the first row, and A and C have all zeroes in the first column. The variable z does not appear in Σ because v and w are both in the chosen fundamental domain. The matrix $\dot{\hat{A}}(z, \lambda)$ is obtained by replacing Σ by a matrix $\dot{\Sigma}$, where $\dot{\Sigma}$ is obtained from $h^{\mathrm{RR}}(\lambda)$ (eq. 8.79) with $\alpha_1 = \alpha_2 = 0$ by switching the first two rows and the first two columns (that is, switching the order of the vertices from (v_1, v, v_2) to (v, v_1, v_2)), to obtain

$$\dot{\Sigma} = \begin{bmatrix} -s\, s_1^{-1} s_2^{-1} & s_1^{-1} & s_2^{-1} \\ s_1^{-1} & -c_1 s_1^{-1} & 0 \\ s_2^{-1} & 0 & -s_2' s_2^{-1} \end{bmatrix}, \tag{8.85}$$

where the relation $s = s_1c_2 + s_1's_2$ is used in the upper left entry.

The 3×3 matrix $K = A - BD^{-1}C$ has all zeroes in its first row and first column. A computation using the relation $T = T_2T_1$ yields the key relation

$$s_1(\lambda)s_2(\lambda)\ \det(\dot{\Sigma} + K)\ =\ s(\lambda)\ \det(\Sigma + K), \tag{8.86}$$

which holds for any matrix K whose first column and and first row vanish. Using this together with

$$\det \hat{\dot{A}} = \det D\ \det(\dot{\Sigma} + K), \qquad \det \hat{A} = \det \hat{\dot{A}} = \det D \det(\Sigma + K) \tag{8.87}$$

yields the statement of the theorem.

If $v_2 = gv_1$ for some $g \in \mathbb{Z}^d$, the process above remains the same, except that

$$\Sigma\ =\ \frac{1}{s}\begin{bmatrix} 1 & 0 \\ 0 & -c - s' + z^g + z^{-g} \end{bmatrix}, \qquad \dot{\Sigma}\ =\ \frac{1}{s_1s_2}\begin{bmatrix} -s & s_2 + z^g s_1 \\ s_2 + z^{-g}s_1 & -c_1s_2 - s_2's_1 \end{bmatrix}, \tag{8.88}$$

and K is a 2×2 matrix with its only nonzero entry being the lower right. In this case, one obtains (8.86) with an extra minus sign on one side. □

Acknowledgement. This material is based upon work supported by the National Science Foundation under Grant No. DMS-1814902.

References

[1] D. S. L. Abergel, V. Apalkov, J. Berashevich, K. Ziegler, and T. Chakraborty. Properties of graphene: a theoretical perspective. *Advances in Physics*, 59(4):261–482, 2010.

[2] S. Albeverio, F. Gesztesy, R. Høegh-Krohn, and H. Holden. *Solvable Models in Quantum Mechanics*. Springer, Heidelberg, 1988.

[3] C. Amovilli, F. E. Leys, and N. H. March. Electronic energy spectrum of two-dimensional solids and a chain of C atoms from a quantum network model. *J. Math. Chem.*, 36:93–112, 2004.

[4] K. Ando, H. Isozaki, E. Korotyaev, and H. Morioka. Inverse scattering on the quantum graph for graphene. *arXiv:2102.05217*, 2021.

[5] C. Bao, W. Yao, E Wang, C. Chen, J. Avila, M. C. Asensio, and S. Zhou. Stacking dependent electronic structure of trilayer graphene resolved by nanospot angle-resolved photoemission spectroscopy. *Nano Lett.*, 17(3):564–1568, 2017.

[6] D. Bättig. *A toroidal compactification of the two-dimensional Bloch-manifold*. PhD thesis, ETH-Zürich, 1988.

[7] D. Bättig. A toroidal compactification of the Fermi surface for the discrete Schrödinger operator. *Comment. Math. Helvetici*, 67:1–16, 1992.

[8] D. Bättig, H. Knörrer, and E. Trubowitz. A directional compactification of the complex Fermi surface. *Compositio Math*, 79(2):205–229, 1991.

[9] S. Becker, R. Han, and S. Jitomirskaya. Cantor spectrum of graphene in magnetic fields. *Inventiones mathematicae*, 218(3):979–1041, 2019.

[10] G. Berkolaiko and A. Comech. Symmetry and Dirac points in graphene spectrum. *J Spect Theor*, 8:1099–1147, 2018.

[11] G. Berkolaiko, J. B. Kennedy, P. Kurasov, and D. Mugnolo. Surgery principles for the spectral analysis of quantum graphs. *Trans. Amer. Math. Soc.*, 372:5153–5197, 2019.

[12] G. Berkolaiko and P. Kuchment. *Introduction to Quantum Graphs*, volume 186 of *Mathematical Surveys and Monographs*. AMS, 2013.

[13] B. M. Brown, K. M. Schmidt, S. P. Shipman, and I. Wood. The inverse problem for a spectral asymmetry function of the Schrödinger operator on a finite interval. *arXiv:2009.03483 [math.SP]*, 2020.

[14] L. C. Campos, T. Taychatanapat, M. Serbyn, K. Surakitbovorn, K. Watanabe, T. Taniguchi, D. A. Abanin, and P. Jarillo-Herrero. Landau level splittings, phase transitions, and nonuniform charge distribution in trilayer graphene. *Phys. Rev. Lett.*, 117:066601, 2016.

[15] E. V. Castro, K. S. Novoselov, S. V. Morozov, N. M. R. Peres, J. M. B. Lopes dos Santos, Johan Nilsson, F. Guinea, A. K. Geim, and A. H. Castro Neto. Biased bilayer graphene: Semiconductor with a gap tunable by the electric field effect. *Phys. Rev. Lett.*, 99:216802, Nov 2007.

[16] A. H. Castro Neto, F. Guinea, N. M. R. Peres, K. S. Novoselov, and A. K. Geim. The electronic properties of graphene. *Rev. Mod. Phys.*, 81:109–162, Jan 2009.

[17] T. Cheon, P. Exner, and O. Turek. Approximation of a general singular vertex coupling in quantum graphs. *Annals of Physics*, 325(3):548 – 578, 2010.

[18] C. A. Coulson. Note on the applicability of the free-electron network model to metals. *Proceedings of the Physical Society. Section A*, 67(7):608–614, jul 1954.

[19] V. L. da Rocha. *Multilayer Graphene through quantum periodic graphs: Dirac cones*. PhD thesis, Universidade Federal de São Carlos, 2020.

[20] C. R. de Oliveira and V. L. Rocha. Dirac cones for bi- and trilayer Bernal-stacked graphene in a quantum graph model. *arXiv:2011.08658*, 2020.

[21] C. R. de Oliveira and V. L. Rocha. Dirac cones for graph models of multilayer AA-stacked graphene sheets. *Z. Naturforsch.*, 76(4):371–384, 2021.

[22] N. T. Do and P. Kuchment. Quantum graph spectra of a graphyne structure. *Nanoscale Systems MMTA*, 2:107–123, 2013.

[23] M. S. P. Eastham. The spectral theory of periodic differential equations. *Scottish Acad. Press. Edinburgh-London*, 1973.

[24] P. Exner, J. P. Keating, P. Kuchment, T. Sunada, and A. Teplayaev, editors. *Analysis on Graphs and its Applications*, volume 77, 2008.

[25] P. Exner and O. Post. Convergence of spectra of graph-like thin manifolds. *J. Geometry and Physics*, 54(1):77–115, 2005.

[26] P. Exner and O. Post. Approximation of quantum graph vertex couplings by scaled Schrödinger operators on thin branched manifolds. *Journal of Physics A: Mathematical and Theoretical*, 42(41):415305, sep 2009.

[27] S. Fan and J. D. Joannopoulos. Analysis of guided resonances in photonic crystal slabs. *Phys. Rev. B*, 65(23):235112–1–8, Jun 2002.

[28] S. Fan, P.R. Villeneuve, and J.D. Joannopoulos. Rate-equation analysis of output efficiency and modulation rate of photonic-crystal light-emitting diodes. *Quantum Electronics, IEEE Journal of*, 36(10):1123–1130, Oct 2000.

[29] U. Fano. Effects of configuration interaction on intensities and phase shifts. *Physical Review*, 124(6):1866–1878, 1961.

[30] C. L. Fefferman and M. I. Weinstein. Honeycomb lattice potentials and Dirac points. *J. AMS*, 25(4):1169–1220, 2012.

[31] D. Gieseker, H. Knörrer, and E. Trubowitz. *The Geometry of Algebraic Fermi Curves*. Academic Press, Boston, 1993.

[32] C. W. Hsu, B. Zhen, S.-L. Chua, S. G. Johnson, J. D. Joannopoulos, and M. Soljacic. Bloch surface eigenstates within the radiation continuum. *Light: Science App.*, 2(e84 doi:10:1038/Isa.2013.40), 2013.

[33] K. S. Kim, A. L. Walter, L. Moreschini, T. Seyller, K. Horn, E. Rotenberg, and A. Bostwick. Coexisting massive and massless Dirac fermions in symmetry-broken bilayer graphene. *Nature Materials*, 12(10):887–892, 2013.

[34] E. Korotyaev and I. Lobanov. Schrödinger operators on zigzag nanotubes. *Ann. Henri Poincaré*, 275(3):805–826, 2007.

[35] E. Korotyaev and I. Lobanov. Zigzag periodic nanotube in magnetic field. *Letters in Mathematical Physics*, 83:83–95, 2008.

[36] P. Kuchment. Graph models for waves in thin structures. *Waves in Random Media*, 12(4):R1–R24, 2002.

[37] P. Kuchment. An overview of periodic elliptic operators. *Bull. Am. Math. Soc.*, 53(3):343–414, 2016.

[38] P. Kuchment and O. Post. On the spectra of carbon nano-structures. *Comm. Math. Phys.*, 275:805–826, 2007.

[39] P. Kuchment and B. Vainberg. On absence of embedded eigenvalues for Schrödinger operators with perturbed periodic potentials. *Commun. Part. Diff. Equat.*, 25(9–10):1809–1826, 2000.

[40] P. Kuchment and B. Vainberg. On the structure of eigenfunctions corresponding to embedded eigenvalues of locally perturbed periodic graph operators. *Comm. Math. Phys.*, 268(3):673–686, 2006.

[41] P. Kuchment and J. Zhao. Analyticity of the spectrum and Dirichlet-to-Neumann operator technique for quantum graphs. *J. Math. Phys.*, 60(093502), 2019.

[42] S. Latil and L. Henrard. Charge carriers in few-layer graphene films. *Phys. Rev. Lett.*, 97:036803, 2006.

[43] F. Leys, C. Amovilli, and N. March. Topology, connectivity, and electronic structure of C and B cages and the corresponding nanotubes. *J. Chem. Inf. Comput. Sci.*, 44(1):122–135, 2004.

[44] W. Li and S. P. Shipman. Irreducibility of the Fermi surface for planar periodic graph operators. *Letters in Mathematical Physics*, 2020.

[45] H. Liu, H. Jiang, and X. C. Xie. Intrinsic superconductivity in ABA-stacked trilayer graphene. *AIP Advances*, 2:041405, 2012.

[46] W. Liu. Irreducibility of the Fermi variety for discrete periodic Schrodinger operators and embedded eigenvalues. *arXiv:2006.04733*, 2020.

[47] E. McCann. Asymmetry gap in the electronic band structure of bilayer graphene. *Phys. Rev. B*, 74:161403, Oct 2006.

[48] E. McCann, D. S. L. Abergel, and V. I. Fal'ko. The low energy electronic band structure of bilayer graphene. *Eur. Phys. J. Special Topics*, 148:91–103, 2007.

[49] E. McCann, D. S. L. Abergel, and V. I. Fal'ko. The low energy electronic band structure of bilayer graphene. *The European Physical Journal Special Topics*, 148(1):91–103, 2007.

[50] H. Niikuni. Spectral band structure of periodic Schrödinger operators with two potentials on the degenerate zigzag nanotube. *J. Appl. Math. Comput.*, 50:453–482, 2016.

[51] B. Partoens and F. M. Peeters. From graphene to graphite: Electronic structure around the K point. *Phys. Rev. B*, 74:075404, Aug 2006.

[52] J. Pöschel and E. Trubowitz. *Inverse Spectral Theory*, volume 130 of *Pure and Applied Mathematics*. Academic Press, 1987.

[53] A. V. Rozhkov, A. O. Sboychakov, A. L. Rakhmanov, and F. Nori. Single-electron gap in the spectrum of twisted bilayer graphene. *Phys. Rev. B*, 95:045119, Jan 2017.

[54] A. V. Rozhkova, A. O. Sboychakova, A. L. Rakhmanova, and F Nori. Electronic properties of graphene-based bilayer systems. *Physics Reports*, 648:1–104, 2016.

[55] K. Ruedenberg and C. W. Scherr. Free-electron network model for conjugated systems. i. theory. *J. Chem. Phys.*, 21, 1953.

[56] A. O. Sboychakov, A. L. Rakhmanov, A. V. Rozhkov, and F. Nori. Electronic spectrum of twisted bilayer graphene. *Phys. Rev. B*, 92:075402, Aug 2015.

[57] J. H. Schenker and M. Aizenman. The creation of spectral gaps by graph decoration. *Lett. Math. Phys.*, 53(3):253–262, 2000.

[58] S. P. Shipman. *Resonant Scattering by Open Periodic Waveguides*, volume 1 of *E-Book, Progress in Computational Physics (Ch. 2)*. Bentham Science Publishers, 2010.

[59] S. P. Shipman. Eigenfunctions of unbounded support for embedded eigenvalues of locally perturbed periodic graph operators. *Comm. Math. Phys.*, 332(2):605–626, 2014.

[60] S. P. Shipman. Reducible Fermi surfaces for non-symmetric bilayer quantum-graph operators. *J. Spectral Theory*, DOI 10.4171/JST/285, 2019.

[61] S. P. Shipman and J. Tillay. Spectra of semi-infinite quantum graph tubes. *Lett. Math. Phys.*, 106:1317–1343, 2016.

[62] S. P. Shipman and S. Venakides. Resonant transmission near non-robust periodic slab modes. *Phys. Rev. E*, 71(1):026611–1–10, 2005.